Diffusion model for Knudsen-type compressor composed of periodic arrays of circular cylinders

Taguchi, Satoshi

(Citation)
PHYSICS OF FLUIDS,22(10):102001-102001

(Issue Date)
2010-10

(Resource Type)
journal article

(Version)
Version of Record

(URL)
https://hdl.handle.net/20.500.14094/90001280

Diffusion model for Knudsen-type compressor composed of periodic arrays of circular cylinders

Satoshi Taguchi[a)]
Organization of Advanced Science and Technology, Kobe University, Kobe 657-8501, Japan

(Received 28 February 2010; accepted 10 September 2010; published online 27 October 2010)

A rarefied gas flow in a long porous channel having a periodic structure that is consisting of alternately arranged porous media and gaps, the former of which contains a periodic array of parallel circular cylinders, is considered for the case in which the channel is infinitely wide. The cylinder arrays have a periodic temperature distribution with the same period as the structure. Under the assumption that the length of each cylinder array and that of each gap are much larger than the period of the cylinders in the array, a fluid-dynamic system describing the overall behavior of the gas in the channel is derived from the kinetic system composed of the Bhatnagar–Gross–Krook equation and the diffuse reflection boundary condition. The derived system is composed of a diffusion model for each cylinder array, whose isothermal version has been reported previously [S. Taguchi and P. Charrier, Phys. Fluids **20**, 067103 (2008)], a set of fluid-dynamic equations for each gap, and the macroscopic connection conditions at each junction between an array and a gap. Then, the fluid-dynamic system is applied to a long channel consisting of many cylinder arrays and gaps. Some numerical results demonstrating the pumping effect of the flow are presented.
 [doi:10.1063/1.3500686]

I. INTRODUCTION

In a rarefied gas or a gas in a small system, a steady flow is produced because of the effect of the temperature field. Such a flow cannot be predicted in the framework of conventional gas dynamics, and therefore, the kinetic theory of gases[1,2] is required for its proper description. Therefore, the study of thermally induced flows is an important area in the field of kinetic theory. As a result, various types of flows, such as the thermal stress slip flow,[3,4] nonlinear thermal stress flow,[4,5] and thermal edge flow,[6,7] have been revealed, in addition to the classical thermal creep flow (or thermal transpiration).[8–19]In addition, various applications of such flows have been proposed. For example, the Knudsen pump (or compressor)[20–35] is driven by the thermal transpiration, whereas the thermal edge pump (or compressor)[36,37] is driven by the thermal edge flow. These devices have an advantage in that they do not contain moving parts.

Another pumping device that has been proposed but has not yet been addressed in the existing literature is the one proposed by Kayashima.[38] This device contains a long porous channel having a periodic structure that is composed of alternately arranged porous media and gaps. The temperature distribution of the channel is also periodic with the same period as the structure. This device is driven by a rarefied gas flow (typically, the thermal transpiration) induced in each nonuniformly heated porous medium. Thus, the basic concept is the same as that of the Knudsen compressor. However, because of its geometrical complexity, this pump has not yet been studied.

Recently, the fundamental flow problems of a rarefied gas through a periodic array of parallel circular cylinders, i.e., the pressure-driven flow[39,40] and temperature-driven flow,[40] have been investigated on the basis of the Bhatnagar–Gross–Krook (BGK) model[41,42] of the Boltzmann equation. It has been shown that a net flow is produced in the direction of the global temperature gradient as long as the Knudsen number based on the molecular mean free path and the period of the cylinders is not very small. Thus, it is possible to develop the device proposed by Kayashima using a periodic array of circular cylinders.

First, we consider the original Knudsen compressor. The typical Knudsen compressor contains a long pipe that is composed of alternately arranged narrow and wide pipes. The temperature distribution of the pipe is also periodic with the same period as the structure. The flow and the pumping effect in this device have been investigated both numerically[23,27] and experimentally.[26,28,29] In real applications, one often has to use a large number of segments. For such a long device, considering the case in which the length of the pipe segment is much larger than the linear dimension of its cross section (e.g., diameter), Aoki *et al.* derived a fluid-dynamic system composed of a diffusion model for each segment and a connection condition at junctions of segments from the Boltzmann system.[31] Such a model can be used as a convenient tool for estimating the properties of the Knudsen pump in various steady and unsteady situations; doing so by a direct numerical analysis or by an experiment is difficult.

Because Kayashima's device and the original Knudsen pump have a similar structure, we can expect that a similar diffusion system can also be obtained for the former by an analysis similar to that performed in Ref. 31. In this study, therefore, we carry out such an analysis. That is, we consider Kayashima's device to be composed of periodic cylinder ar-

a)Electronic mail: taguchi@mech.kobe-u.ac.jp.

rays and derive a diffusion model for each cylinder array and a set of fluid-dynamic equations for each gap, together with the connection condition at each junction of an array and a gap, under the condition that the length of each array and gap is much larger than the period of the cylinders in the array.

Some simplifications are introduced in this paper. First, we consider the case of an infinitely wide channel and neglect the effect of the channel wall (i.e., the flow is considered to be globally one dimensional). Second, we employ the BGK model of the Boltzmann equation and the diffuse reflection boundary condition on the cylinder surface as our basic kinetic system. This choice greatly simplifies the analysis because we can make use of some existing results. On the other hand, some disadvantages of the BGK model have also been noted in literature. The main disadvantage is that this model gives the Prandtl number fixed to unity, whereas for real monatomic gases, it is approximately 2/3. Consequently, the viscosity and thermal conductivity of the gas cannot be simultaneously adjusted to the corresponding values of a real gas, and this may cause a difficulty when comparing the result with experimental data. However, it is expected that the derived model will describe the qualitative behavior of the flow with sufficient accuracy. It should also be noted that the method itself can be applied to other kinetic models, as well as to the original Boltzmann equation, and the consequence arises only in the transport properties of the model that emerge in the transport coefficients. These coefficients can be obtained through additional computational efforts.

The remainder of this paper is organized as follows. In Sec. II, we consider a flow through a vast extent of a periodic array of parallel circular cylinders with a global temperature distribution. Under the assumption that the length scale of variation of the global temperature distribution is much larger than the period of the cylinders, a diffusion model that describes the global pressure distribution of the gas and the mass flux in the array is derived from the kinetic system by homogenization.[43] The diffusion model contains two transport coefficients that are essentially given by the mass-flow rates of the pressure- and temperature-driven flows that have been obtained in the previous studies. Next, in Sec. III, we consider a flow across a gap and investigate its overall behavior. Under the assumption that the distance across the gap is much larger than the mean free path of the gas molecules (or the Knudsen number is small), we derive a set of fluid-dynamic equations describing the flow by a standard asymptotic analysis of the BGK equation for small Knudsen numbers.[2,44–48] In Sec. IV, we consider the case in which a cylinder array is in contact with a half space filled with the gas and investigate the behavior of the gas flowing through the cylinder array to the half space. Here, the purpose is to derive the connection conditions at the junction of the cylinder array and the gap for the diffusion model and the fluid-dynamic equations derived in Secs. II and III, respectively. Then, we briefly revisit the pressure- and temperature-driven flows and present the numerical values of the transport coefficients contained in the diffusion model in Sec. V. The system of the diffusion model, the fluid-dynamic equations, and the connection conditions derived in this manner are summarized in Sec. VI, and the numerical result is presented in Sec. VII. We consider a flow through a long (and wide) porous channel composed of alternately repeated cylinder arrays and gaps. We numerically investigate the pressure distribution and the mass-flow rate in the structure on the basis of the fluid-dynamic system derived in Secs. II–IV. Section VIII presents the conclusions.

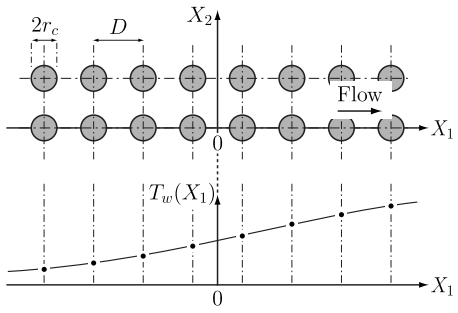

FIG. 1. A rarefied gas flow past a square array of parallel circular cylinders. T_w describes the overall distribution of the cylinder temperatures and each cylinder temperature is indicated by •.

II. FLOW PAST A SQUARE ARRAY OF CIRCULAR CYLINDERS AND ITS FLUID-DYNAMIC MODEL

A. Problem and basic equations

Let us consider a rarefied gas flow past a periodic square array of parallel circular cylinders (see Fig. 1). We take the X_3 axis parallel to the cylinders and let the centers of cylinders be located on the lattice points $(X_1,X_2)=((m+1/2)D,nD)$ $(m,n=0,\pm 1,\pm 2,\ldots)$, where D is the distance between the centers of neighboring cylinders (or the period of the cylinders). The common radius of the cylinders is $r_c(<D/2)$. The temperature of the cylinders, which is constant in time and uniform in the row $X_1=$const, has a distribution in the X_1 direction described by $T_w(X_1)$ $(-\infty<X_1<\infty)$. More specifically, the temperature of the cylinders in the row $X_1=(m+1/2)D$, which we denote by T_{wm}, is given by $T_{wm}=T_w((m+1/2)D)$. Let us denote by L the characteristic length scale of variation of T_w. We investigate the behavior of the gas induced around the cylinders under the following assumptions:

(i) The behavior of the gas is described by the BGK model of the Boltzmann equation.
(ii) The gas molecules leaving the cylinder surface obey the diffuse reflection condition.
(iii) The characteristic length scale of variation of the cylinder temperatures is much larger than the cylinder period, i.e., $L \gg D$.

Let t denote the time variable, ξ_i (or $\boldsymbol{\xi}$) the molecular velocity, $f(X_1,X_2,\boldsymbol{\xi},t)$ the velocity distribution function, ρ the density, v_i $(v_3=0)$ the flow velocity, T the temperature, and p the pressure of the gas. The BGK equation describing the behavior of the gas is written, in the present two-dimensional problem, as

$$\frac{\partial f}{\partial t} + \xi_1 \frac{\partial f}{\partial X_1} + \xi_2 \frac{\partial f}{\partial X_2} = A_c \rho (f_e - f), \tag{1}$$

$$f_e = \frac{\rho}{(2\pi RT)^{3/2}} \exp\left(- \frac{(\xi_j - v_j)^2}{2RT} \right), \tag{2}$$

$$\rho = \int f d\boldsymbol{\xi}, \tag{3}$$

$$v_i = \frac{1}{\rho} \int \xi_i f d\boldsymbol{\xi}, \tag{4}$$

$$p = R\rho T = \frac{1}{3} \int (\xi_j - v_j)^2 f d\boldsymbol{\xi}, \tag{5}$$

where R is the specific gas constant (the Boltzmann constant divided by the mass of a molecule), A_c is a constant ($A_c\rho$ is the collision frequency), and $d\boldsymbol{\xi}=d\xi_1 d\xi_2 d\xi_3$. Here and in what follows, the domain of integration with respect to $\boldsymbol{\xi}$ is the whole space, unless otherwise stated. The summation convention is assumed for double indices throughout the paper.

The diffuse reflection boundary condition on the cylinder surface is written in the following form:

$$f = \frac{\sigma_w}{(2\pi RT_{wm})^{3/2}} \exp\left(- \frac{\xi_j^2}{2RT_{wm}} \right) \quad \text{for } \xi_j n_j > 0 \quad \text{on } S^*_{mn}, \tag{6}$$

with

$$\sigma_w = - \left(\frac{2\pi}{RT_{wm}} \right)^{1/2} \int_{\xi_j n_j < 0} \xi_j n_j f d\boldsymbol{\xi}. \tag{7}$$

Here, S^*_{mn} denotes the surface of the cylinder with its center at $(X_1, X_2) = ((m+1/2)D, nD)$ in the (X_1, X_2) plane and n_i $(n_3=0)$ is the unit normal vector to S^*_{mn} pointing to the gas. It is noted that there is no mass flux across the surface (the impermeability condition), i.e.,

$$\int \xi_j n_j f d\boldsymbol{\xi} = 0. \tag{8}$$

In addition, an initial condition should be prescribed, i.e.,

$$f(X_1, X_2, \boldsymbol{\xi}, 0) = f^0(X_1, X_2, \boldsymbol{\xi}). \tag{9}$$

B. Scaling

We are interested in the solution whose length scale of variation is L in the X_1 direction (the direction in which the cylinder temperature varies), which is much larger than D (the period of the cylinders) [see assumption (iii) in Sec. II A]. For this purpose, let us introduce the following dimensionless variables:

$$\hat{t} = \frac{t}{t_*}, \quad y = \frac{X_1}{L}, \quad x_2 = \frac{X_2}{D},$$

$$\zeta_i = \frac{\xi_i}{(2RT_*)^{1/2}}, \quad \hat{f} = \frac{f}{\rho_* / (2RT_*)^{3/2}},$$

$$\hat{\rho} = \frac{\rho}{\rho_*}, \quad \hat{v}_i = \frac{v_i}{(2RT_*)^{1/2}}, \quad \hat{T} = \frac{T}{T_*}, \tag{10}$$

$$\hat{p} = \frac{p}{p_*}, \quad (\hat{T}_{wm}, \hat{T}_w) = \frac{(T_{wm}, T_w)}{T_*},$$

$$\hat{r}_c = \frac{r_c}{D}.$$

Here, t_*, ρ_*, T_*, and $p_* = R\rho_* T_*$ are the reference time, the reference density, the reference temperature, and the reference pressure, respectively. Note that $\hat{v}_3 = 0$. Hereafter, we assume that the flow field is periodic in x_2 with period 1 (or D in the dimensional X_2 variable) and consider the problem in the domain $-\infty < x_1 < \infty$ and $-1/2 \leqslant x_2 \leqslant 1/2$ by imposing the periodic boundary conditions at $x_2 = \pm 1/2$. With these new variables, the BGK equation (1) is recast as

$$S_* \frac{\partial \hat{f}}{\partial \hat{t}} + \epsilon \zeta_1 \frac{\partial \hat{f}}{\partial y} + \zeta_2 \frac{\partial \hat{f}}{\partial x_2} = \frac{2}{\sqrt{\pi}} \frac{1}{K_*} \hat{\rho} (\hat{f}_e - \hat{f}), \tag{11}$$

$$\hat{f}_e = \frac{\hat{\rho}}{(\pi \hat{T})^{3/2}} \exp\left(- \frac{(\zeta_j - \hat{v}_j)^2}{\hat{T}} \right), \tag{12}$$

$$\hat{\rho} = \int \hat{f} d\boldsymbol{\zeta}, \tag{13}$$

$$\hat{v}_i = \frac{1}{\hat{\rho}} \int \zeta_i \hat{f} d\boldsymbol{\zeta}, \tag{14}$$

$$\hat{p} = \hat{\rho}\hat{T} = \frac{2}{3} \int (\zeta_j - \hat{v}_j)^2 \hat{f} d\boldsymbol{\zeta}, \tag{15}$$

$$d\boldsymbol{\zeta} = d\zeta_1 d\zeta_2 d\zeta_3. \tag{16}$$

Here and in what follows, the domain of integration with respect to $\boldsymbol{\zeta} = (\zeta_1, \zeta_2, \zeta_3)$ is the whole space, unless otherwise stated. The dimensionless parameters S_*, K_*, and ϵ are defined by

$$S_* = \frac{D}{t_* (2RT_*)^{1/2}}, \quad K_* = \frac{\ell_*}{D}, \quad \epsilon = \frac{D}{L}, \tag{17}$$

where $\ell_* = (2/\sqrt{\pi})(2RT_*)^{1/2} / A_c \rho_*$ is the mean free path of the gas molecules in the equilibrium state at rest with density ρ_* and temperature T_*. ℓ_* is related to the corresponding viscosity μ_* by $\mu_* = (\sqrt{\pi}/2) p_* (2RT_*)^{-1/2} \ell_*$. (Thus, the constant A_c can be expressed as $A_c = p_* / \rho_* \mu_*$.) S_* and K_* are the Strouhal number and the Knudsen number, respectively. S_* is specified later together with the reference time t_*.

The dimensionless form of the boundary condition is given by

$$\hat{f} = \frac{\hat{\sigma}_w}{(\pi \hat{T}_{wm})^{3/2}} \exp\left(-\frac{\zeta_j^2}{\hat{T}_{wm}}\right) \quad \text{for} \quad \zeta_j n_j > 0, \quad \text{on} \quad S_m \quad (m = 0, \pm 1, \pm 2, \ldots), \tag{18}$$

$$\hat{\sigma}_w = -2\left(\frac{\pi}{\hat{T}_{wm}}\right)^{1/2} \int_{\zeta_j n_j < 0} \zeta_j n_j \hat{f} d\boldsymbol{\zeta}, \tag{19}$$

$$\hat{f}: \text{periodic} \quad (x_2 = \pm 1/2). \tag{20}$$

Here, S_m represents the location of the cylinder surface with its center at $(y, x_2) = (\epsilon(m+1/2), 0)$ in the (y, x_2) plane and n_i $(n_3 = 0)$ is the unit vector on S_m radially directed from the center. It should be noted that since the length scale of variation of T_w is L, its dimensionless counterpart $\hat{T}_w$ is a function of y, i.e., $\hat{T}_w = \hat{T}_w(y)$. Therefore, the relation between the (dimensionless) cylinder temperature $\hat{T}_{wm}$ and $\hat{T}_w$ (Sec. II A) should be written as

$$\hat{T}_{wm} = \hat{T}_w(\epsilon(m + 1/2)) \quad (m = 0, \pm 1, \pm 2, \ldots). \tag{21}$$

Finally, the dimensionless initial condition reads as

$$\hat{f}(y, x_2, \boldsymbol{\zeta}, 0) = \hat{f}^0(y, x_2, \boldsymbol{\zeta}), \tag{22}$$

where $\hat{f}^0(y, x_2, \boldsymbol{\zeta}) = (2RT_*)^{3/2} \rho_*^{-1} f^0(X_1, X_2, \boldsymbol{\zeta})$.

Because of the assumption of the slow variation in the cylinder temperature [assumption (iii) in Sec. II A], ϵ is a small parameter. In this situation, the flow induced around cylinders by the thermal effect is expected to be small. Therefore, we assume that the characteristic flow speed is of the order of $(2RT_*)^{1/2}\epsilon$. In this case, the corresponding reference time may be taken as $t_* = L/(2RT_*)^{1/2}\epsilon$, and the resulting Strouhal number is ϵ^2, i.e.,

$$S_* = \frac{D}{t_*(2RT_*)^{1/2}} = \frac{D}{L/\epsilon} = \epsilon^2. \tag{23}$$

On the other hand, we assume that K_* is of the order of unity. To summarize, the BGK equation to be solved is given by

$$\epsilon^2 \frac{\partial \hat{f}}{\partial \hat{t}} + \epsilon \zeta_1 \frac{\partial \hat{f}}{\partial y} + \zeta_2 \frac{\partial \hat{f}}{\partial x_2} = \frac{2}{\sqrt{\pi}} \frac{1}{K_*} \hat{\rho}(\hat{f}_e - \hat{f}). \tag{24}$$

C. Homogenization

In this section, we try to obtain the solution to Eqs. (24) and (12)–(15) subject to the boundary conditions (18)–(20) by homogenization.[43] That is, we introduce a new space variable,

$$x_1 = y/\epsilon = X_1/D, \tag{25}$$

and assume that (i) $\hat{f}$ depends not only on y but also on x_1 in the direction of the global temperature variation, i.e.,

$$\hat{f} = \hat{f}(y, x_1, x_2, \boldsymbol{\zeta}, \hat{t}), \tag{26}$$

and (ii) $\hat{f}$ is periodic in x_1 with period 1. The variable y describes the long scale variation over the distance across which the cylinder temperature varies appreciably, whereas the variable x_1 corresponds to the short scale variation over the period of the cylinders. With this new $\hat{f}$, Eq. (24) is recast as

$$\epsilon^2 \frac{\partial \hat{f}}{\partial \hat{t}} + \epsilon \zeta_1 \frac{\partial \hat{f}}{\partial y} + \zeta_1 \frac{\partial \hat{f}}{\partial x_1} + \zeta_2 \frac{\partial \hat{f}}{\partial x_2} = \frac{2}{\sqrt{\pi}} \frac{1}{K_*} \hat{\rho}(\hat{f}_e - \hat{f}). \tag{27}$$

We seek the solution $\hat{f}$ in the form of expansion in the small parameter ϵ, i.e.,

$$\hat{f} = \hat{f}_{(0)} + \hat{f}_{(1)}\epsilon + \hat{f}_{(2)}\epsilon^2 + \cdots. \tag{28}$$

Correspondingly, the macroscopic quantities of the gas h $(h = \hat{\rho}, \hat{v}_1, \hat{v}_2, \hat{T}$, and $\hat{p})$ are expanded in ϵ as

$$h = h_{(0)} + h_{(1)}\epsilon + h_{(2)}\epsilon^2 + \cdots. \tag{29}$$

The relations between $h_{(m)}$ and $\hat{f}_{(m)}$ are obtained by substituting the expansions of h and $\hat{f}$ into the definition of the macroscopic quantities [Eqs. (13)–(15)] and equating the coefficients of the same power of ϵ. We also expand the local Maxwellian $\hat{f}_e$ in ϵ, i.e.,

$$\hat{f}_e = \hat{f}_{e(0)} + \hat{f}_{e(1)}\epsilon + \hat{f}_{e(2)}\epsilon^2 + \cdots. \tag{30}$$

If we substitute Eqs. (28)–(30) into Eqs. (27) and (18)–(20) and take into account the following expansion of $\hat{T}_{wm}$ around $y(=\epsilon x_1)$:

$$\hat{T}_{wm} = \hat{T}_w + \frac{d\hat{T}_w}{dy}\left(m + \frac{1}{2} - x_1\right)\epsilon + \frac{1}{2}\frac{d^2\hat{T}_w}{dy^2}\left(m + \frac{1}{2} - x_1\right)^2\epsilon^2 + \cdots, \tag{31}$$

we obtain a sequence of boundary-value problems for $\hat{f}_{(m)}$, which can be solved from the lowest order.

1. Problem for ϵ^0 order

The equation and the boundary condition for the zeroth order in ϵ are given by

$$\zeta_1 \frac{\partial \hat{f}_{(0)}}{\partial x_1} + \zeta_2 \frac{\partial \hat{f}_{(0)}}{\partial x_2} = \frac{2}{\sqrt{\pi}} \frac{1}{K_*} \hat{\rho}_{(0)}(\hat{f}_{e(0)} - \hat{f}_{(0)}) \quad (\mathbf{x} \in X_f), \tag{32}$$

$$\hat{f}_{e(0)} = \frac{\hat{\rho}_{(0)}}{(\pi \hat{T}_{(0)})^{3/2}} \exp\left(-\frac{(\zeta_j - \hat{v}_{j(0)})^2}{\hat{T}_{(0)}}\right), \tag{33}$$

$$\hat{f}_{(0)} = \frac{\hat{\sigma}_{w(0)}}{[\pi \hat{T}_w(y)]^{3/2}} \exp\left(-\frac{\zeta_j^2}{\hat{T}_w(y)}\right) \quad \text{for} \quad \zeta_j n_j > 0 \quad (\mathbf{x} \in S), \tag{34}$$

$$\hat{\sigma}_{w(0)} = -2\left(\frac{\pi}{\hat{T}_w(y)}\right)^{1/2} \int_{\zeta_j n_j < 0} \zeta_j n_j \hat{f}_{(0)} d\boldsymbol{\zeta}, \tag{35}$$

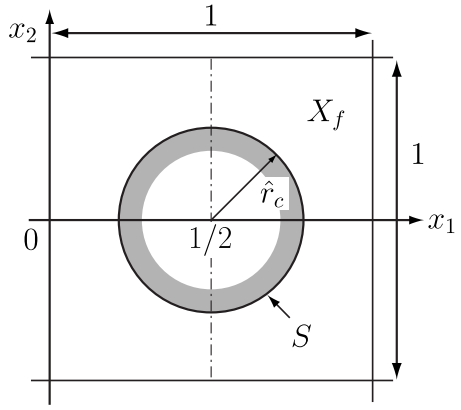

FIG. 2. A unit cell in the (x_1,x_2) plane.

$$\hat{f}_{(0)}\text{: periodic} \quad (x_1=0,1,x_2=\pm 1/2), \tag{36}$$

where $\hat{v}_{3(0)}=0$. Here, $\mathbf{x}=(x_1,x_2)$ is the two-dimensional position vector in the (x_1,x_2) plane, X_f is the gas region in the unit cell with a square shape bounded by $x_1=0$ and 1 and $x_2=\pm 1/2$, S is the location of the cylinder surface with radius $\hat{r}_c$ centered at $(x_1,x_2)=(1/2,0)$ in the unit cell, and n_i is the unit normal vector to S pointing to the gas (see Fig. 2). The zeroth order macroscopic quantities $\hat{\rho}_{(0)}$, $\hat{v}_{1(0)}$, $\hat{v}_{2(0)}$, $\hat{T}_{(0)}$, and $\hat{p}_{(0)}$ are expressed in terms of $\hat{f}_{(0)}$ as

$$\hat{\rho}_{(0)}=\int \hat{f}_{(0)}d\boldsymbol{\zeta}, \tag{37a}$$

$$\hat{v}_{i(0)}=\frac{1}{\hat{\rho}_{(0)}}\int \zeta_i\hat{f}_{(0)}d\boldsymbol{\zeta}, \tag{37b}$$

$$\hat{p}_{(0)}=\hat{\rho}_{(0)}\hat{T}_{(0)}=\frac{2}{3}\int (\zeta_j-\hat{v}_{j(0)})^2\hat{f}_{(0)}d\boldsymbol{\zeta}. \tag{37c}$$

It should be noted that the variables y and $\hat{t}$ enter this system only as parameters. Because of this property and the periodicity of $\hat{f}$ in x_1 (and in x_2), the problem is reduced to the boundary-value problems (32)–(36) in the unit cell.

It can be easily seen that the following Maxwellian:

$$\hat{f}_{(0)}=\frac{\varrho_{(0)}(y,\hat{t})}{[\pi\hat{T}_w(y)]^{3/2}}\exp\left(-\frac{\zeta_j^2}{\hat{T}_w(y)}\right), \tag{38}$$

which is independent of $\mathbf{x}$, satisfies Eqs. (32)–(36) with Eq. (37). Here, $\varrho_{(0)}$ is an arbitrary function of y and $\hat{t}$. This is also the unique solution.[33,43] If we substitute Eq. (38) into Eq. (37), we obtain

$$\hat{\rho}_{(0)}=\varrho_{(0)}, \quad \hat{v}_{i(0)}=0, \tag{39a}$$

$$\hat{T}_{(0)}=\hat{p}_{(0)}/\hat{\rho}_{(0)}=\hat{T}_w(y). \tag{39b}$$

Thus, the zeroth order solution is written as

$$\hat{f}_{(0)}=\frac{\hat{\rho}_{(0)}(y,\hat{t})}{[\pi\hat{T}_w(y)]^{3/2}}\exp\left(-\frac{\zeta_j^2}{\hat{T}_w(y)}\right), \tag{40}$$

with an undetermined $\hat{\rho}_{(0)}$.

2. Problem for ϵ^1 order

With the aid of the solution $\hat{f}_{(0)}$ to the zeroth order problem, the equation and boundary condition for the first order in ϵ are given by

$$\zeta_1\frac{\partial\hat{f}_{(1)}}{\partial x_1}+\zeta_2\frac{\partial\hat{f}_{(1)}}{\partial x_2}=\frac{2}{\sqrt{\pi}}\frac{1}{K_*}\hat{\rho}_{(0)}(\hat{f}_{e(1)}-\hat{f}_{(1)})-\zeta_1\frac{\partial\hat{f}_{(0)}}{\partial y} \quad (\mathbf{x}\in X_f), \tag{41}$$

$$\hat{f}_{e(1)}=\hat{f}_{(0)}\left[\frac{\hat{\rho}_{(1)}}{\hat{\rho}_{(0)}}+2\frac{\hat{v}_{1(1)}}{\hat{T}_w}\zeta_1+2\frac{\hat{v}_{2(1)}}{\hat{T}_w}\zeta_2+\left(\frac{\zeta_j^2}{\hat{T}_w}-\frac{3}{2}\right)\frac{\hat{T}_{(1)}}{\hat{T}_w}\right], \tag{42}$$

$$\hat{f}_{(1)}=\hat{f}_{(0)}\left[\frac{\hat{\sigma}_{w(1)}}{\hat{\rho}_{(0)}}-\left(\frac{\zeta_j^2}{\hat{T}_w}-\frac{3}{2}\right)\frac{1}{\hat{T}_w}\frac{d\hat{T}_w}{dy}\left(x_1-\frac{1}{2}\right)\right] \quad \text{for } \zeta_jn_j>0 \quad (\mathbf{x}\in S), \tag{43}$$

$$\hat{\sigma}_{w(1)}=-2\left(\frac{\pi}{\hat{T}_w}\right)^{1/2}\int_{\zeta_jn_j<0}\zeta_jn_j\hat{f}_{(1)}d\boldsymbol{\zeta}+\frac{\hat{\rho}_{(0)}}{2}\frac{1}{\hat{T}_w}\frac{d\hat{T}_w}{dy}\left(x_1-\frac{1}{2}\right), \tag{44}$$

$$\hat{f}_{(1)}\text{: periodic} \quad (x_1=0,1,x_2=\pm 1/2). \tag{45}$$

The first order macroscopic quantities $\hat{\rho}_{(1)}$, $\hat{v}_{1(1)}$, $\hat{v}_{2(1)}$, $\hat{T}_{(1)}$, and $\hat{p}_{(1)}$ are given by

$$\hat{\rho}_{(1)}=\int \hat{f}_{(1)}d\boldsymbol{\zeta}, \tag{46a}$$

$$\hat{v}_{i(1)}=\frac{1}{\hat{\rho}_{(0)}}\int \zeta_i\hat{f}_{(1)}d\boldsymbol{\zeta}, \tag{46b}$$

$$\hat{p}_{(1)}=\hat{\rho}_{(0)}\hat{T}_{(1)}+\hat{\rho}_{(1)}\hat{T}_w=\frac{2}{3}\int \zeta_j^2\hat{f}_{(1)}d\boldsymbol{\zeta}. \tag{46c}$$

Equation (41) is the linearized BGK equation with the inhomogeneous term

$$-\zeta_1\frac{\partial\hat{f}_{(0)}}{\partial y}=-\zeta_1\hat{f}_{(0)}\left[\frac{\partial\ln\hat{p}_{(0)}}{\partial y}+\left(\frac{\zeta_j^2}{\hat{T}_w}-\frac{5}{2}\right)\frac{d\ln\hat{T}_w}{dy}\right]. \tag{47}$$

Because of the linearity of the problem and the forms of the inhomogeneous terms, we can seek the solution in the form,

$$\hat{f}_{(1)} = \hat{f}_{(0)}\left[\phi_P(\mathbf{x},\mathbf{c};K(y,\hat{t}),\hat{r}_c)\frac{\partial \ln \hat{p}_{(0)}}{\partial y} + \phi_T(\mathbf{x},\mathbf{c};K(y,\hat{t}),\hat{r}_c)\frac{d \ln \hat{T}_w}{dy}\right], \tag{48}$$

$$\mathbf{c} = (c_1,c_2,c_3), \quad c_i = \frac{\zeta_i}{\hat{T}_w^{1/2}}, \tag{49}$$

where K is a kind of local Knudsen number defined by

$$K = \frac{K_*[\hat{T}_w(y)]^{1/2}}{\hat{\rho}_{(0)}(y,\hat{t})} = \frac{K_*[\hat{T}_w(y)]^{3/2}}{\hat{p}_{(0)}(y,\hat{t})}, \tag{50}$$

and ϕ_P and ϕ_T are the solutions of the following boundary-value problems:

$$c_1\frac{\partial \phi_\alpha}{\partial x_1} + c_2\frac{\partial \phi_\alpha}{\partial x_2} = \frac{2}{\sqrt{\pi}}\frac{1}{K}\hat{L}_{\mathrm{BGK}}(\phi_\alpha) - I_\alpha \quad (\mathbf{x}\in X_f), \tag{51}$$

$$\phi_\alpha = \kappa_{w\alpha} + \left(c^2 - \tfrac{3}{2}\right)\tau_{w\alpha} \quad \text{for } c_j n_j > 0 \quad (\mathbf{x}\in S), \tag{52}$$

$$\kappa_{w\alpha} = -2\sqrt{\pi}\int_{c_j n_j<0} c_j n_j \phi_\alpha E(\mathbf{c})d\mathbf{c} - \frac{1}{2}\tau_{w\alpha}, \tag{53}$$

$$\phi_\alpha\text{: periodic} \quad (x_1 = 0,1, x_2 = \pm 1/2), \tag{54}$$

$$E(\mathbf{c}) = \pi^{-3/2}\exp(-c^2), \tag{55}$$

$$d\mathbf{c} = dc_1 dc_2 dc_3, \quad c = |\mathbf{c}|. \tag{56}$$

Here, $\alpha = P$ and T,

$$I_P = c_1, \quad I_T = c_1(c^2 - 5/2), \tag{57}$$

$$\tau_{wP} = 0, \quad \tau_{wT} = -(x_1 - 1/2), \tag{58}$$

and $\hat{L}_{\mathrm{BGK}}$ is the linearized BGK collision operator defined by

$$\hat{L}_{\mathrm{BGK}}(g) = \int\left[1 + 2(c_1c_{1*} + c_2c_{2*}) + \frac{2}{3}\left(c_j^2 - \frac{3}{2}\right)\left(c_{j*}^2 - \frac{3}{2}\right)\right] \times g(\mathbf{c}_*)E(\mathbf{c}_*)d\mathbf{c}_* - g, \tag{59}$$

where g is a function of $\mathbf{c}$ and c_{i*} (or $\mathbf{c}_*$) is the variable of integration corresponding to c_i. It should be noted that ϕ_P and ϕ_T depend on K and $\hat{r}_c$ (through S) and K depends on y and $\hat{t}$. These dependencies are explicitly shown in Eq. (48).

Equations (51)–(54) are equivalent to the equation and boundary condition for the two fundamental flow problems of a rarefied gas associated with a periodic array of cylinders. More precisely, let us consider a rarefied gas flow over infinitely many parallel circular cylinders with a square array arrangement, driven by a (small) uniform pressure gradient or by a (small) uniform temperature gradient, whose direction is perpendicular to a plane containing a row of cylinders. If we consider these problems on the basis of the linearized BGK equation with the diffuse reflection condition on the boundaries, ϕ_P and ϕ_T of Eqs. (51)–(54) correspond to the solution of the pressure-driven flow and that of the temperature-driven flow, respectively. These problems have been studied in Ref. 39 (the pressure-driven flow) and in Ref. 40 (the pressure- and temperature-driven flows). We will come back to this point later in Sec. V.

By substituting Eq. (48) into Eq. (46), the first order macroscopic quantities in ϵ are expressed in the following forms:

$$\hat{\rho}_{(1)} = \hat{\rho}_{(0)}\left(\omega_P\frac{\partial \ln \hat{p}_{(0)}}{\partial y} + \omega_T\frac{d \ln \hat{T}_w}{dy}\right), \tag{60a}$$

$$\hat{v}_{i(1)} = \hat{T}_w^{1/2}\left(u_{iP}\frac{\partial \ln \hat{p}_{(0)}}{\partial y} + u_{iT}\frac{d \ln \hat{T}_w}{dy}\right), \tag{60b}$$

$$\hat{T}_{(1)} = \hat{T}_w\left(\tau_P\frac{\partial \ln \hat{p}_{(0)}}{\partial y} + \tau_T\frac{d \ln \hat{T}_w}{dy}\right), \tag{60c}$$

$$\hat{p}_{(1)} = \hat{p}_{(0)}\left(P_P\frac{\partial \ln \hat{p}_{(0)}}{\partial y} + P_T\frac{d \ln \hat{T}_w}{dy}\right), \tag{60d}$$

where ω_α, $u_{i\alpha}$ ($u_{3\alpha}=0$), τ_α, and P_α are defined by

$$\omega_\alpha(\mathbf{x};K,\hat{r}_c) = \int \phi_\alpha(\mathbf{c},\mathbf{x};K,\hat{r}_c)E(\mathbf{c})d\mathbf{c}, \tag{61a}$$

$$u_{i\alpha}(\mathbf{x};K,\hat{r}_c) = \int c_i\phi_\alpha(\mathbf{c},\mathbf{x};K,\hat{r}_c)E(\mathbf{c})d\mathbf{c}, \tag{61b}$$

$$\tau_\alpha(\mathbf{x};K,\hat{r}_c) = (2/3)\int (c^2 - 3/2)\phi_\alpha(\mathbf{c},\mathbf{x};K,\hat{r}_c)E(\mathbf{c})d\mathbf{c}, \tag{61c}$$

$$P_\alpha(\mathbf{x};K,\hat{r}_c) = \omega_\alpha + \tau_\alpha. \tag{61d}$$

It may be noted that ω_α, $u_{i\alpha}$, τ_α, and P_α depend on y and $\hat{t}$ through K.

3. Problem for ϵ^2 order and diffusion model

Now we consider the problem for the second order in ϵ. The equation and boundary conditions for $\hat{f}_{(2)}$ are given by

$$\zeta_1\frac{\partial \hat{f}_{(2)}}{\partial x_1} + \zeta_2\frac{\partial \hat{f}_{(2)}}{\partial x_2} = \frac{2}{\sqrt{\pi}}\frac{1}{K_*}[\hat{\rho}_{(0)}(\hat{f}_{e(2)} - \hat{f}_{(2)}) + \hat{\rho}_{(1)}(\hat{f}_{e(1)} - \hat{f}_{(1)})] - \frac{\partial \hat{f}_{(0)}}{\partial \hat{t}} - \zeta_1\frac{\partial \hat{f}_{(1)}}{\partial y} \quad (\mathbf{x}\in X_f), \tag{62}$$

$$\hat{f}_{e(2)} = \cdots,$$

$$\hat{f}_{(2)} = \cdots \quad \text{for } \zeta_j n_j > 0 \quad (\mathbf{x}\in S),$$

$$\hat{f}_{(2)}\text{: periodic} \quad (x_1 = 0,1, x_2 = \pm 1/2), \tag{63}$$

where the explicit form of $\hat{f}_{e(2)}$ and that of the boundary condition on the cylinder surface S are omitted. In this subsection, we do not solve this problem but derive a fluid-

dynamic model from the necessary condition in order for the problem to have a solution.

We first integrate Eq. (62) with respect to $\boldsymbol{\zeta}$ over the whole space. Since the contribution from the collision term vanishes, this yields

$$\frac{\partial \hat{\rho}_{(0)}}{\partial \hat{t}} + \frac{\partial}{\partial y}(\hat{\rho}_{(0)}\hat{v}_{1(1)}) = -\left(\frac{\partial}{\partial x_1}\int \zeta_1 \hat{f}_{(2)} d\boldsymbol{\zeta} + \frac{\partial}{\partial x_2}\int \zeta_2 \hat{f}_{(2)} d\boldsymbol{\zeta}\right). \tag{64}$$

Here, Eqs. (37a) and (46b) have been used. Since $\hat{\rho}_{(0)}$ does not depend on $\mathbf{x}$, further integration with respect to x_1 and x_2 over X_f in the unit cell gives

$$(1-\pi \hat{r}_c^2)\frac{\partial \hat{\rho}_{(0)}}{\partial \hat{t}} + \frac{\partial}{\partial y}\left(\hat{\rho}_{(0)}\int_{X_f} \hat{v}_{1(1)} d\mathbf{x}\right) = -\int_{X_f}\left(\frac{\partial}{\partial x_1}\int \zeta_1 \hat{f}_{(2)} d\boldsymbol{\zeta} + \frac{\partial}{\partial x_2}\int \zeta_2 \hat{f}_{(2)} d\boldsymbol{\zeta}\right) d\mathbf{x}, \tag{65}$$

where $d\mathbf{x}=dx_1 dx_2$. The right-hand side of the above equation is shown to be zero with the aid of the divergence theorem and the periodic condition (63), as well as the impermeability condition on the cylinder surface, i.e.,

$$\int \zeta_j n_j \hat{f}_{(2)} d\boldsymbol{\zeta} = 0 \quad (\mathbf{x} \in S) \tag{66}$$

[cf. Eq. (8)]. Thus, Eq. (65) is rewritten, with the aid of Eq. (60b), in the following form:

$$(1-\pi \hat{r}_c^2)\frac{\partial \hat{\rho}_{(0)}}{\partial \hat{t}} + \frac{\partial}{\partial y}\left[\hat{\rho}_{(0)}\hat{T}_w^{1/2}\left(\mathcal{M}_P \frac{\partial \ln \hat{p}_{(0)}}{\partial y} + \mathcal{M}_T \frac{d \ln \hat{T}_w}{dy}\right)\right] = 0, \tag{67}$$

where $\mathcal{M}_P$ and $\mathcal{M}_T$ are defined by

$$\mathcal{M}_\alpha(K,\hat{r}_c) = \int_{X_f} u_{1\alpha}(\mathbf{x};K,\hat{r}_c) d\mathbf{x} \quad (\alpha = P,T). \tag{68}$$

We note that the integral $\int_{-1/2}^{1/2} u_{1\alpha}|_{x_1=\text{const}} dx_2$ is independent of x_1. Here, the integrand should be interpreted to be zero inside the cylinder (this kind of remark will not be repeated below since no confusion is expected). Therefore, Eq. (68) is further transformed into

$$\mathcal{M}_\alpha(K,\hat{r}_c) = \int_{-1/2}^{1/2} u_{1\alpha}(\mathbf{x};K,\hat{r}_c)|_{x_1=\text{const}} dx_2. \tag{69}$$

Here, $\mathcal{M}_P$ and $\mathcal{M}_T$ are the dimensionless mass-flow rate in the x_1 direction of the pressure-driven flow and that of the temperature-driven flow, respectively [see the paragraph after Eq. (59)]. Multiplying Eq. (67) by $\hat{T}_w(y)$, we obtain the equation for $\hat{p}_{(0)}$ [Eq. (39b)], which is summarized as follows:

$$\frac{\partial \hat{p}_{(0)}}{\partial \hat{t}} + \frac{\hat{T}_w}{(1-\pi \hat{r}_c^2)}\frac{\partial M}{\partial y} = 0, \tag{70a}$$

$$M = \frac{\hat{p}_{(0)}}{\hat{T}_w^{1/2}}\left[\mathcal{M}_P(K,\hat{r}_c)\frac{\partial \ln \hat{p}_{(0)}}{\partial y} + \mathcal{M}_T(K,\hat{r}_c)\frac{d \ln \hat{T}_w}{dy}\right], \tag{70b}$$

$$K = K_* \hat{T}_w^{3/2}/\hat{p}_{(0)}. \tag{70c}$$

Here, we note that the variable M corresponds to the dimensionless mass-flow rate in the y (or X_1) direction. That is, if we denote by $\tilde{M}$ the total mass-flow rate (per unit time) across the plane $X_1=\text{const}$ with unit length in X_3 and with length D in the X_2 direction, $\tilde{M}$ is related to M by the relation

$$\frac{\tilde{M}}{\rho_*(2RT_*)^{1/2}D} = \epsilon M + O(\epsilon^2). \tag{71}$$

Equation (70) is a (nonlinear) drift-diffusion equation for $\hat{p}_{(0)}$ with the transport coefficients $\mathcal{M}_P$ and $\mathcal{M}_T$. If we specify appropriate initial and boundary conditions, it describes the transient behavior of the overall pressure distribution and mass flux of the gas in the cylinder array with a finite length.

A very similar model has been derived for a long pipe in Ref. 31 under the condition of the smallness of the linear dimension of its cross section compared to the longitudinal length of the pipe. Its extension to the case of a curved channel,[33] as well as to the case of a gas mixture,[49] has also been made. On the other hand, such models have been frequently used in literature to analyze microflow problems.[50–53] An attempt to apply the present model to more realistic porous media has been made in Ref. 54. It should also be mentioned that the diffusion approximation for a periodic array of parallel circular cylinders has been made mathematically rigorous for a Knudsen (or free-molecular) gas.[55]

III. FLOW ACROSS A GAP AND ITS FLUID-DYNAMIC EQUATIONS

In Sec. II, we have investigated the global behavior of the flow through a cylinder array, without regard to the presence of the gaps beside it. In this section, in turn, we consider the global behavior of the flow across the gap. We recall that the mean free path of the gas molecules has been assumed to be comparable to the period of the cylinders in the array [see the sentence following Eq. (23)]. Therefore, if the distance across the gap is large compared to the cylinder period, the Knudsen number based on the mean free path and the size of the gap is small, and the behavior of the gas will be described in a fluid-dynamic manner. In addition, the flow speed is also small since the flow produced in the array is weak [Eq. (71)]. Motivated by these observations, we will consider the following problem.

A. Problem

Consider a one-dimensional rarefied gas flow parallel to the X_1 axis (i.e., $v_2=v_3=0$). Let us denote by ρ_* the reference density, by T_* the reference temperature, and by ℓ_* the mean free path of the gas molecules in the equilibrium state at rest with density ρ_* and temperature T_*. The length scale of variation of fluid variables is denoted by L. We investigate the behavior of the gas based on the BGK equation under the following assumptions: (i) the length scale of variation L is much larger than the mean free path ℓ_*, or the Knudsen number $\mathrm{Kn}=\ell_*/L$ is small; and (ii) the flow speed is small and the Mach number is of the same order as the Knudsen number Kn.

For the sake of later convenience, we introduce length D which is of the same order as the mean free path, i.e., $D\sim\ell_*$. Then, using the same dimensionless variables and the time scale introduced in Sec. II B, the BGK equation describing the flow is written as

$$\epsilon^2\frac{\partial\hat{f}}{\partial\hat{t}}+\epsilon\zeta_1\frac{\partial\hat{f}}{\partial y}=\frac{2}{\sqrt{\pi}}\frac{1}{K_*}\hat{\rho}(\hat{f}_e-\hat{f}), \tag{72}$$

$$\hat{f}_e=\frac{\hat{\rho}}{(\pi\hat{T})^{3/2}}\exp\left(-\frac{(\zeta_j-\hat{v}_1\delta_{j1})^2}{\hat{T}}\right). \tag{73}$$

Here, $\hat{\rho}$, $\hat{v}_1$, and $\hat{T}$ are given by Eqs. (13)–(15), δ_{ij} is the Kronecker delta, and ϵ and K_* are the same as those defined in Eq. (17) (i.e., $\epsilon=D/L$ and $K_*=\ell_*/D$). Since $\mathrm{Kn}=K_*\epsilon$, ϵ is a small parameter which is of the same order as Kn. We will carry out below an asymptotic analysis of Eq. (72) for small ϵ under the condition

$$|\hat{v}_1|=O(\epsilon), \tag{74}$$

[assumption (ii) in this section].

B. Asymptotic analysis and fluid-dynamic equations

In this subsection, we obtain the solution of Eq. (72). Since the corresponding asymptotic analysis for the Boltzmann equation under condition (74) is explained in detail in literature (see, e.g., Refs. 2, 47, and 48), we briefly summarize the outline of the analysis and present the result.

We seek the solution $\hat{f}$ of Eq. (72) in the form of expansion in ϵ, i.e.,

$$\hat{f}=\hat{f}_{(0)}+\hat{f}_{(1)}\epsilon+\hat{f}_{(2)}\epsilon^2+\cdots. \tag{75}$$

Accordingly, the macroscopic quantities are expanded in ϵ as

$$h=h_{(0)}+h_{(1)}\epsilon+h_{(2)}\epsilon^2+\cdots \quad (\text{for } h=\hat{\rho},\hat{T}, \text{ and } \hat{p}), \tag{76a}$$

$$\hat{v}_1=\hat{v}_{1(1)}\epsilon+\hat{v}_{1(2)}\epsilon^2+\cdots. \tag{76b}$$

Here, the expansion of $\hat{v}_1$ is started from ϵ order (i.e., $\hat{v}_{1(0)}\equiv 0$) to meet condition (74). The local Maxwellian is also expanded in ϵ, i.e.,

$$\hat{f}_e=\hat{f}_{e(0)}+\hat{f}_{e(1)}\epsilon+\hat{f}_{e(2)}\epsilon^2+\cdots. \tag{77}$$

Substitution of Eqs. (75)–(77) into Eq. (72) yields a recursive expression for $\hat{f}_{(m)}$ $(m=0,1,\ldots)$ with $\hat{f}_{(0)}$ given by

$$\hat{f}_{(0)}=\frac{\hat{\rho}_{(0)}(y,\hat{t})}{[\pi\hat{T}_{(0)}(y,\hat{t})]^{3/2}}\exp\left(-\frac{\zeta_j^2}{\hat{T}_{(0)}(y,\hat{t})}\right), \tag{78}$$

where $\hat{\rho}_{(0)}$ and $\hat{T}_{(0)}$ are undetermined functions of y and $\hat{t}$. On the other hand, from the property of the collision term, the following compatibility conditions must be satisfied:

$$\int\psi_r\zeta_1\frac{\partial\hat{f}_{(0)}}{\partial y}d\boldsymbol{\zeta}=0, \tag{79a}$$

$$\int\psi_r\left(\zeta_1\frac{\partial\hat{f}_{(m)}}{\partial y}+\frac{\partial\hat{f}_{(m-1)}}{\partial\hat{t}}\right)d\boldsymbol{\zeta}=0 \quad (m\geqslant 1), \tag{79b}$$

where ψ_r denotes the collision invariants, i.e., $\psi_0=1$, $\psi_r=\zeta_r$ $(r=1,2,3)$, and $\psi_4=\zeta_j^2$. Substituting $\hat{f}_{(0)}$ and $\hat{f}_{(m)}$ $(m\geqslant 1)$ successively obtained from $\hat{f}_{(0)}$ into Eq. (79), we obtain sets of partial differential equations governing $\hat{\rho}_{(n)}$, $\hat{v}_{1(n+1)}$, and $\hat{T}_{(n)}$ $(n\geqslant 0)$ (the fluid-dynamic equations).

Here, we give the explicit form of the leading order set of the fluid-dynamic equations as well as that of $\hat{f}_{(1)}$ thus obtained. The equations are summarized as

$$\frac{\partial\hat{p}_{(0)}}{\partial y}=0, \tag{80a}$$

$$\frac{\partial\hat{\rho}_{(0)}}{\partial\hat{t}}+\frac{\partial}{\partial y}(\hat{\rho}_{(0)}\hat{v}_{1(1)})=0, \tag{80b}$$

$$\frac{3}{2}\frac{\partial\hat{p}_{(0)}}{\partial\hat{t}}+\frac{\partial}{\partial y}\left(\frac{5}{2}\hat{p}_{(0)}\hat{v}_{1(1)}-\frac{5}{4}k_*\hat{T}_{(0)}\frac{\partial\hat{T}_{(0)}}{\partial y}\right)=0, \tag{80c}$$

$$\hat{p}_{(0)}=\hat{\rho}_{(0)}\hat{T}_{(0)}, \tag{80d}$$

where

$$k_*=\frac{\sqrt{\pi}}{2}K_*. \tag{81}$$

$\hat{f}_{(1)}$ is given by

$$\hat{f}_{(1)}=\hat{f}_{(0)}\left[\frac{\hat{p}_{(1)}}{\hat{p}_{(0)}}+2\frac{\zeta_1}{\hat{T}_{(0)}}\hat{v}_{1(1)}+\left(\frac{\zeta_j^2}{\hat{T}_{(0)}}-\frac{5}{2}\right)\frac{\hat{T}_{(1)}}{\hat{T}_{(0)}}-\zeta_1\left(\frac{\zeta_j^2}{\hat{T}_{(0)}}-\frac{5}{2}\right)\frac{k_*}{\hat{p}_{(0)}}\frac{\partial\hat{T}_{(0)}}{\partial y}\right]. \tag{82}$$

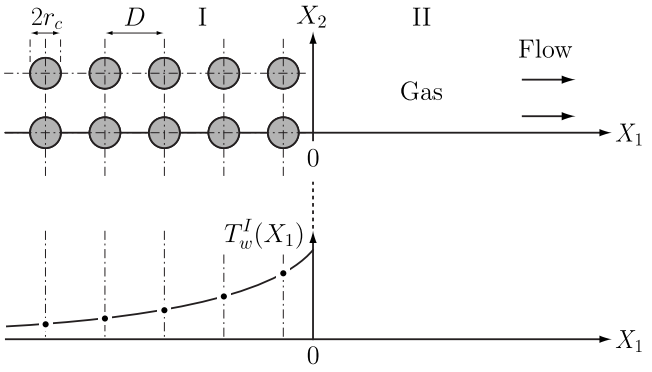

FIG. 3. A square array of circular cylinders in contact with a half space. T_w^I describes the overall distribution of the cylinder temperatures and each cylinder temperature is indicated by •.

IV. CYLINDER ARRAY IN CONTACT WITH A HALF SPACE

In this section, we consider the case in which a cylinder array is in contact with a half space filled with the gas and discuss the flow in the array and the half space on the basis of the diffusion model and the fluid-dynamic equations derived in Secs. II and III, respectively.

A. Connection problem

Let two semi-infinite domains, domain I ($X_1<0$) with a square array of circular cylinders and domain II ($X_1\geqslant 0$) without cylinders, be joined at $X_1=0$ (see Fig. 3). In domain I, the centers of the cylinders are located on the lattice points $(X_1,X_2)=((m+1/2)D,nD)$ $(m=-1,-2,-3,\ldots;n=0,\pm 1,\pm 2,\ldots)$ in the (X_1,X_2) plane, with D being the distance between the centers of adjacent cylinders. The radius of the cylinders is commonly r_c. As in Sec. II, the global distribution of the cylinder temperatures is described by $T_w^{\mathrm{I}}(X_1)$ $(-\infty<X_1<0)$, that is, the temperature of the cylinders in the row $X_1=(m+1/2)D$ is given by $T_{wm}^{\mathrm{I}}=T_w^{\mathrm{I}}((m+1/2)D)$. Since both domains I and II are large, the behavior of the gas in domain I and that in domain II are described by the diffusion model derived in Sec. II and by the fluid-dynamic equations derived in Sec. III, respectively, with a local correction near the junction. In this section, we investigate this correction and derive the connection condition for the diffusion model and the fluid-dynamic equations at the junction.

We assume the periodicity of the flow field in X_2 with period D and use again the same dimensionless variables as in Sec. II B to nondimensionalize the present problem. Let us denote the solution by F instead of $\hat{f}$. We also denote by $\hat{T}_{wm}^{\mathrm{I}}$ and $\hat{T}_w^{\mathrm{I}}$ the dimensionless counterparts of T_{wm}^{I} and T_w^{I}, respectively. Then, the equation and boundary conditions become as follows. The BGK equation is

$$\epsilon^2\frac{\partial F}{\partial \hat{t}}+\epsilon\zeta_1\frac{\partial F}{\partial y}+\zeta_2\frac{\partial F}{\partial x_2}=\frac{2}{\sqrt{\pi}}\frac{1}{K_*}\hat{\rho}(F_e-F), \tag{83}$$

$$F_e=\frac{\hat{\rho}}{(\pi\hat{T})^{3/2}}\exp\left[-\frac{(\zeta_j-\hat{v}_j)^2}{\hat{T}}\right], \tag{84}$$

$$\hat{\rho}=\int F d\boldsymbol{\zeta}, \tag{85a}$$

$$\hat{v}_i=\frac{1}{\hat{\rho}}\int \zeta_i F d\boldsymbol{\zeta}, \tag{85b}$$

$$\hat{p}=\hat{\rho}\hat{T}=\frac{2}{3}\int(\zeta_i-\hat{v}_i)^2 F d\boldsymbol{\zeta}, \tag{85c}$$

where $\hat{v}_3=0$, and the boundary conditions are

$$F=\frac{\hat{\sigma}_w^{\mathrm{I}}}{(\pi\hat{T}_{wm}^{\mathrm{I}})^{3/2}}\exp\left(-\frac{\zeta_j^2}{\hat{T}_{wm}^{\mathrm{I}}}\right)\quad\text{for}\quad \zeta_j n_j>0,\quad \text{on}\quad S_m^{\mathrm{I}}\quad (m=-1,-2,\ldots), \tag{86}$$

$$\hat{\sigma}_w^{\mathrm{I}}=-2\left(\frac{\pi}{\hat{T}_{wm}^{\mathrm{I}}}\right)^{1/2}\int_{\zeta_j n_j<0}\zeta_j n_j F d\boldsymbol{\zeta}, \tag{87}$$

$$F\text{: periodic}\quad (x_2=\pm 1/2). \tag{88}$$

Here, S_m^{I} represents the location of the cylinder surface with its center at $(y,x_2)=(\epsilon(m+1/2),0)$ in the (y,x_2) plane and n_i $(n_3=0)$ is the unit vector on S_m^{I} radially directed from the center. By the same reasoning as in Sec. II B [see the paragraph containing Eq. (21)], $\hat{T}_w^{\mathrm{I}}$ is a function of y only and $\hat{T}_{wm}^{\mathrm{I}}$ is given by

$$\hat{T}_{wm}^{\mathrm{I}}=\hat{T}_w^{\mathrm{I}}(\epsilon(m+1/2))\quad (m=-1,-2,\ldots). \tag{89}$$

Finally, the range of x_2 in the above system is $-1/2\leqslant x_2\leqslant 1/2$.

Now, we denote by F^{I} the restriction of F in domain I ($F^{\mathrm{I}}=F$ for $-\infty<y<0$) and by F^{II} that of F in domain II ($F^{\mathrm{II}}=F$ for $0\leqslant y<\infty$). Then, F^{I} satisfies Eqs. (83)–(85) and the boundary conditions (86)–(88), whereas F^{II} satisfies Eqs. (83)–(85) and the boundary condition (88). Moreover, since F should be continuous at the junction ($y=0$), F^{I} and F^{II} satisfy the following continuity condition:[56]

$$F^{\mathrm{I}}(y=0_-,x_2,\boldsymbol{\zeta},\hat{t})=F^{\mathrm{II}}(y=0,x_2,\boldsymbol{\zeta},\hat{t})\quad (-1/2\leqslant x_2\leqslant 1/2). \tag{90}$$

B. Condition at junction

Let us first assume that F^{I} and F^{II} are given by the corresponding restrictions of $\hat{f}$ obtained in Secs. II and III, respectively. More precisely, we assume that F^{I} is given by the solution $\hat{f}$ of (24) and (18)–(20) with $\hat{T}_{wm}=\hat{T}_{wm}^{\mathrm{I}}$ and F^{II} is given by the solution $\hat{f}$ of Eq. (72). We denote such F^J by F_f^J $(J=\mathrm{I},\mathrm{II})$. Then, $F_f^{\mathrm{I}}=F_f^{\mathrm{I}}(y,x_1,x_2,\boldsymbol{\zeta},\hat{t})$ with $x_1=y/\epsilon$ and $F_f^{\mathrm{II}}=F_f^{\mathrm{II}}(y,\boldsymbol{\zeta},\hat{t})$ are expanded in ϵ as

$$F_f^J=F_{f(0)}^J+F_{f(1)}^J\epsilon+F_{f(2)}^J\epsilon^2+\cdots\quad (J=\mathrm{I},\mathrm{II}). \tag{91}$$

For example, $F_{f(0)}^{\mathrm{I}}$ and $F_{f(0)}^{\mathrm{II}}$ are given by the following Maxwellians [cf. Eqs. (40) and (78)]:

$$F^{\mathrm{I}}_{f(0)} = \frac{\hat{\rho}^{\mathrm{I}}_{(0)}(y,\hat{t})}{[\pi \hat{T}^{\mathrm{I}}_{w}(y)]^{3/2}} \exp\left(- \frac{\zeta_j^2}{\hat{T}^{\mathrm{I}}_{w}(y)} \right), \tag{92a}$$

$$F^{\mathrm{II}}_{f(0)} = \frac{\hat{\rho}^{\mathrm{II}}_{(0)}(y,\hat{t})}{[\pi \hat{T}^{\mathrm{II}}_{(0)}(y,\hat{t})]^{3/2}} \exp\left(- \frac{\zeta_j^2}{\hat{T}^{\mathrm{II}}_{(0)}(y,\hat{t})} \right), \tag{92b}$$

where $\hat{\rho}^{\mathrm{I}}_{(0)}$, $\hat{\rho}^{\mathrm{II}}_{(0)}$, and $\hat{T}^{\mathrm{II}}_{(0)}$ are undetermined functions.

At the zeroth order in ϵ, it is easily checked that the above $F^{\mathrm{I}}_{f(0)}$ and $F^{\mathrm{II}}_{f(0)}$ satisfy the equation and boundary condition for F^{I} and F^{II}, respectively. In addition, if we impose the conditions

$$\hat{\rho}^{\mathrm{I}}_{(0)}(y=0\_,\hat{t}) = \hat{\rho}^{\mathrm{II}}_{(0)}(y=0,\hat{t}), \tag{93a}$$

$$\hat{T}^{\mathrm{I}}_{w}(y=0\_) = \hat{T}^{\mathrm{II}}_{(0)}(y=0,\hat{t}), \tag{93b}$$

or, equivalently,

$$\hat{p}^{\mathrm{I}}_{(0)}(y=0\_,\hat{t}) = \hat{p}^{\mathrm{II}}_{(0)}(y=0,\hat{t}), \tag{94a}$$

$$\hat{T}^{\mathrm{I}}_{w}(y=0\_) = \hat{T}^{\mathrm{II}}_{(0)}(y=0,\hat{t}), \tag{94b}$$

where $\hat{p}^{\mathrm{I}}_{(0)}=\hat{\rho}^{\mathrm{I}}_{(0)}\hat{T}^{\mathrm{I}}_{w}$ and $\hat{p}^{\mathrm{II}}_{(0)}=\hat{\rho}^{\mathrm{II}}_{(0)}\hat{T}^{\mathrm{II}}_{(0)}$, the continuity condition at the kinetic level (90) is also satisfied.

At the first order in ϵ, $F^{\mathrm{I}}_{f(1)}$ is the corresponding restriction of $\hat{f}_{(1)}$ of Eq. (48) with $\hat{T}_w=\hat{T}^{\mathrm{I}}_{w}$ and $F^{\mathrm{II}}_{f(1)}$ is that of Eq. (82). However, for these $F^{\mathrm{I}}_{f(1)}$ and $F^{\mathrm{II}}_{f(1)}$, the continuity condition (90) cannot be made to satisfy since $F^{\mathrm{I}}_{f(1)}$ depends on x_2 but $F^{\mathrm{II}}_{f(1)}$ does not. Therefore, we seek the restriction F^J satisfying Eq. (90) in the form

$$F^J = F^J_f + G^J, \tag{95}$$

where G^J is a correction term only appreciable near the junction. We assume that G^J is a function of $x_1(=y/\epsilon)$, x_2, $\boldsymbol{\zeta}$, and $\hat{t}$, i.e.,

$$G^J = G^J(x_1,x_2,\boldsymbol{\zeta},\hat{t}), \tag{96}$$

and that G^J is periodic in x_2 with period 1. Note that G^I is defined for $-\infty<x_1<0$ and G^{II} for $0\leqslant x_1<\infty$. Corresponding to Eq. (91), G^J is sought in the form of expansion in ϵ,

$$G^J = G^J_{(1)}\epsilon + G^J_{(2)}\epsilon^2 + \cdots, \tag{97}$$

where the expansion is started from the first order since the continuity condition is already satisfied by $F^J_{f(0)}$. If we substitute Eq. (95) with Eqs. (91) and (97) into the original equation and boundary conditions for F^J, and take into account the properties of F^J_f as well as those for G^J, we obtain the equation and boundary conditions for the coefficients $G^J_{(m)}$ $(m=1,2,\ldots)$. Here, we summarize the equation and boundary conditions for $G^J_{(1)}$ thus obtained. The equation is

$$\zeta_1 \frac{\partial G^J_{(1)}}{\partial x_1} + \zeta_2 \frac{\partial G^J_{(1)}}{\partial x_2} = \frac{2}{\sqrt{\pi}} \frac{(\hat{\rho}^I_{(0)})^-}{K_*} \left\{ (F^I_{f(0)})^- \left[\frac{\hat{\rho}^J_{G(1)}}{(\hat{\rho}^I_{(0)})^-} + 2\frac{\zeta_1}{(\hat{T}^I_w)^-}\hat{v}^J_{1G(1)} + 2\frac{\zeta_2}{(\hat{T}^I_w)^-}\hat{v}^J_{2G(1)} + \left(\frac{\zeta_j^2}{(\hat{T}^I_w)^-} - \frac{3}{2} \right) \frac{\hat{T}^J_{G(1)}}{(\hat{T}^I_w)^-} \right] - G^J_{(1)} \right\}, \tag{98}$$

where $(\cdot)^-$ indicates the value at $y=0\_$, $\hat{\rho}^J_{G(1)}$, $\hat{v}^J_{iG(1)}$ $(\hat{v}^J_{3G(1)}=0)$, and $\hat{T}^J_{G(1)}$ are, respectively, the density, flow velocity, and temperature of the gas corresponding to $G^J_{(1)}$ that are defined by

$$\hat{\rho}^J_{G(1)} = \int G^J_{(1)} d\boldsymbol{\zeta}, \tag{99a}$$

$$\hat{v}^J_{iG(1)} = \frac{1}{(\hat{\rho}^I_{(0)})^-} \int \zeta_i G^J_{(1)} d\boldsymbol{\zeta}, \tag{99b}$$

$$\hat{T}^J_{G(1)} = \frac{2}{3}\frac{(\hat{T}^I_w)^-}{(\hat{\rho}^I_{(0)})^-} \int \left(\frac{\zeta_j^2}{(\hat{T}^I_w)^-} - \frac{3}{2} \right) G^J_{(1)} d\boldsymbol{\zeta}, \tag{99c}$$

and relation (93) has been used. The boundary condition for $G^{\mathrm{I}}_{(1)}$ in domain I $(-\infty<x_1<0)$ and that for $G^{\mathrm{II}}_{(1)}$ in domain II $(0\leqslant x_1<\infty)$ are

$$G^{\mathrm{I}}_{(1)} = \frac{\hat{\sigma}^{\mathrm{I}}_{wG(1)}}{[\pi(\hat{T}^{\mathrm{I}}_{w})^-]^{3/2}} \exp\left(- \frac{\zeta_j^2}{(\hat{T}^{\mathrm{I}}_{w})^-} \right) \quad \text{for} \quad \zeta_j n_j > 0, \quad \text{on} \quad \bar{S}_m \quad (m=-1,-2,\ldots), \tag{100}$$

$$\hat{\sigma}^{\mathrm{I}}_{wG(1)} = -2\left(\frac{\pi}{(\hat{T}^{\mathrm{I}}_{w})^-} \right)^{1/2} \int_{\zeta_j n_j<0} \zeta_j n_j G^{\mathrm{I}}_{(1)} d\boldsymbol{\zeta}, \tag{101}$$

$$G^{\mathrm{I}}_{(1)} \text{ and } G^{\mathrm{II}}_{(1)}\text{: periodic} \quad (x_2 = \pm 1/2), \tag{102}$$

where $\bar{S}_m$ represents the location of the cylinder surface with radius $\hat{r}_c$ centered at $(x_1,x_2)=(m+1/2,0)$ in the (x_1,x_2) plane and n_i $(n_3=0)$ is the unit normal vector to $\bar{S}_m$ pointing to the gas. The continuity condition at the junction $(x_1=0)$ reads as

$$F^{\mathrm{I}}_{f(1)}(y=0\_,x_1=0\_,x_2,\boldsymbol{\zeta},\hat{t}) + G^{\mathrm{I}}_{(1)}(x_1=0\_,x_2,\boldsymbol{\zeta},\hat{t}) = F^{\mathrm{II}}_{f(1)}(y=0,\boldsymbol{\zeta},\hat{t}) + G^{\mathrm{II}}_{(1)}(x_1=0,x_2,\boldsymbol{\zeta},\hat{t}). \tag{103}$$

Finally, since $G^J_{(1)}$ is a correction, the following conditions are imposed:

$$G^{\mathrm{I}}_{(1)} \to 0 \quad (\text{as } x_1 \to -\infty), \tag{104}$$

$$G^{\mathrm{II}}_{(1)} \to 0 \quad (\text{as } x_1 \to \infty). \tag{105}$$

In the present study, we admit the existence of the solution to Eqs. (98)–(105) and derive the connection condition for $F^{\mathrm{I}}_{f(1)}$ and $F^{\mathrm{II}}_{f(1)}$.

First, the integration of Eq. (98) over the whole space of $\boldsymbol{\zeta}$ gives

$$\frac{\partial}{\partial x_1}\int \zeta_1 G^J_{(1)} d\boldsymbol{\zeta} + \frac{\partial}{\partial x_2}\int \zeta_2 G^J_{(1)} d\boldsymbol{\zeta} = 0. \tag{106}$$

Now we integrate Eq. (106) with $J=\mathrm{I}$ with respect to x_1 and x_2 over the domain bounded by $x_1=0$, $x_1=c^{\mathrm{I}}$ ($c^{\mathrm{I}}<0$:const), $x_2=\pm 1/2$, and by the boundaries of the cylinders. If we denote such a domain by D^{I}, then

$$\int_{D^{\mathrm{I}}} \left(\frac{\partial}{\partial x_1}\int \zeta_1 G^{\mathrm{I}}_{(1)} d\boldsymbol{\zeta} + \frac{\partial}{\partial x_2}\int \zeta_2 G^{\mathrm{I}}_{(1)} d\boldsymbol{\zeta} \right) d\mathbf{x} = 0. \tag{107}$$

By using the divergence theorem and the periodic condition (102) for $G^{\mathrm{I}}_{(1)}$, as well as the fact that Eqs. (100) and (101) give $\int \zeta_i n_i G^{\mathrm{I}}_{(1)} d\boldsymbol{\zeta}=0$ on the cylinder surface, this reduces to

$$\int_{-1/2}^{1/2}\int \zeta_1 G^{\mathrm{I}}_{(1)}|_{x_1=0_-} d\boldsymbol{\zeta} dx_2 = \int_{-1/2}^{1/2}\int \zeta_1 G^{\mathrm{I}}_{(1)}|_{x_1=c^{\mathrm{I}}} d\boldsymbol{\zeta} dx_2. \tag{108}$$

By letting $c^{\mathrm{I}}\to -\infty$ and using condition (104), we obtain

$$\int_{-1/2}^{1/2}\int \zeta_1 G^{\mathrm{I}}_{(1)}(x_1=0_-, x_2, \boldsymbol{\zeta}, \hat{t}) d\boldsymbol{\zeta} dx_2 = 0. \tag{109}$$

Similarly, integrating Eq. (106) with $J=\mathrm{II}$ with respect to x_1 and x_2 over the domain bounded by $x_1=0$, $x_1=c^{\mathrm{II}}$ ($c^{\mathrm{II}}>0$:const), and $x_2=\pm 1/2$, and using the divergence theorem as well as the periodic condition (102) for $G^{\mathrm{II}}_{(1)}$, we find a relation for $G^{\mathrm{II}}_{(1)}$ corresponding to Eq. (108). Then, letting $c^{\mathrm{II}}\to\infty$ and using condition (105), we obtain

$$\int_{-1/2}^{1/2}\int \zeta_1 G^{\mathrm{II}}_{(1)}(x_1=0, x_2, \boldsymbol{\zeta}, \hat{t}) d\boldsymbol{\zeta} dx_2 = 0. \tag{110}$$

On the other hand, multiplying the continuity condition (103) by ζ_1 and integrating the result over the whole space of $\boldsymbol{\zeta}$, and further integration with respect to x_2 from $-1/2$ to $1/2$ give

$$\int_{-1/2}^{1/2}\int \zeta_1 F^{\mathrm{I}}_{f(1)}|^{y=0_-}_{x_1=0_-} d\boldsymbol{\zeta} dx_2 + \int_{-1/2}^{1/2}\int \zeta_1 G^{\mathrm{I}}_{(1)}|_{x_1=0_-} d\boldsymbol{\zeta} dx_2 = \int \zeta_1 F^{\mathrm{II}}_{f(1)}|_{y=0} d\boldsymbol{\zeta} + \int_{-1/2}^{1/2}\int \zeta_1 G^{\mathrm{II}}_{(1)}|_{x_1=0} d\boldsymbol{\zeta} dx_2, \tag{111}$$

where the fact that $F^{\mathrm{II}}_{f(1)}$ is independent of x_2 has been used. But, since Eqs. (109) and (110) hold, this reduces to

$$\int_{-1/2}^{1/2}\int \zeta_1 F^{\mathrm{I}}_{f(1)}(y=0_-, x_1=0_-, x_2, \boldsymbol{\zeta}, \hat{t}) d\boldsymbol{\zeta} dx_2 = \int \zeta_1 F^{\mathrm{II}}_{f(1)}(y=0, \boldsymbol{\zeta}, \hat{t}) d\boldsymbol{\zeta}. \tag{112}$$

We now recall that $F^{\mathrm{I}}_{f(1)}$ is the restriction for $y<0$ of the solution $\hat{f}_{(1)}$ obtained in Sec. II with $\hat{T}_w=\hat{T}^{\mathrm{I}}_w$ and that $F^{\mathrm{II}}_{f(1)}$ is the restriction for $y\geqslant 0$ of the solution $\hat{f}_{(1)}$ obtained in Sec. III. Therefore, we have, from Eqs. (46b), (60b), and (69),

$$\int_{-1/2}^{1/2}\int \zeta_1 F^{\mathrm{I}}_{f(1)} d\boldsymbol{\zeta} dx_2 = M^{\mathrm{I}}, \tag{113}$$

$$M^{\mathrm{I}} = \frac{\hat{p}^{\mathrm{I}}_{(0)}}{(\hat{T}^{\mathrm{I}}_w)^{1/2}}\left[\mathcal{M}_P(K^{\mathrm{I}}, \hat{r}_c)\frac{\partial \ln \hat{p}^{\mathrm{I}}_{(0)}}{\partial y} + \mathcal{M}_T(K^{\mathrm{I}}, \hat{r}_c)\frac{d \ln \hat{T}^{\mathrm{I}}_w}{dy} \right], \tag{114}$$

$$K^{\mathrm{I}} = \frac{K_*(\hat{T}^{\mathrm{I}}_w)^{3/2}}{\hat{p}^{\mathrm{I}}_{(0)}}, \tag{115}$$

and from Eq. (82),

$$\int \zeta_1 F^{\mathrm{II}}_{f(1)} d\boldsymbol{\zeta} = \hat{\rho}^{\mathrm{II}}_{(0)}\hat{v}^{\mathrm{II}}_{1(1)}. \tag{116}$$

With Eqs. (113) and (116), Eq. (112) becomes

$$M^{\mathrm{I}}|_{y=0_-} = (\hat{\rho}^{\mathrm{II}}_{(0)}\hat{v}^{\mathrm{II}}_{1(1)})|_{y=0}. \tag{117}$$

To summarize, the zeroth order pressure $\hat{p}^{\mathrm{I}}_{(0)}$ in domain I and the zeroth order density $\hat{\rho}^{\mathrm{II}}_{(0)}$, pressure $\hat{p}^{\mathrm{II}}_{(0)}$, temperature $\hat{T}^{\mathrm{II}}_{(0)}$, and the first order flow velocity $\hat{v}^{\mathrm{II}}_{1(1)}$ in domain II are described by the following equations and connection conditions:

$$\frac{\partial \hat{p}^{\mathrm{I}}_{(0)}}{\partial \hat{t}} + \frac{\hat{T}^{\mathrm{I}}_w}{(1-\pi\hat{r}_c^2)}\frac{\partial M^{\mathrm{I}}}{\partial y} = 0, \tag{118}$$

$$\frac{\partial \hat{p}^{\mathrm{II}}_{(0)}}{\partial y} = 0, \tag{119a}$$

$$\frac{\partial \hat{\rho}^{\mathrm{II}}_{(0)}}{\partial \hat{t}} + \frac{\partial}{\partial y}(\hat{\rho}^{\mathrm{II}}_{(0)}\hat{v}^{\mathrm{II}}_{1(1)}) = 0, \tag{119b}$$

$$\frac{3}{2}\frac{\partial \hat{p}^{\mathrm{II}}_{(0)}}{\partial \hat{t}} + \frac{\partial}{\partial y}\left(\frac{5}{2}\hat{p}^{\mathrm{II}}_{(0)}\hat{v}^{\mathrm{II}}_{1(1)} - \frac{5}{4}k_*\hat{T}^{\mathrm{II}}_{(0)}\frac{\partial \hat{T}^{\mathrm{II}}_{(0)}}{\partial y} \right) = 0, \tag{119c}$$

$$\hat{\rho}^{\mathrm{II}}_{(0)} = \hat{p}^{\mathrm{II}}_{(0)}/\hat{T}^{\mathrm{II}}_{(0)}, \tag{119d}$$

$$\hat{p}^{\mathrm{I}}_{(0)}|_{y=0_-} = \hat{p}^{\mathrm{II}}_{(0)}|_{y=0_+}, \tag{120a}$$

$$\hat{T}^{\mathrm{I}}_w|_{y=0_-} = \hat{T}^{\mathrm{II}}_{(0)}|_{y=0_+}, \tag{120b}$$

$$M^{\mathrm{I}}|_{y=0_-} = (\hat{\rho}^{\mathrm{II}}_{(0)}\hat{v}^{\mathrm{II}}_{1(1)})|_{y=0_+}, \tag{120c}$$

where M^{I} is given by Eq. (114) and $y=0$ on the right-hand sides of Eqs. (94) and (117) has been replaced by $y=0_+$.

V. FLOW AROUND PARALLEL CIRCULAR CYLINDERS INDUCED BY SMALL PRESSURE AND TEMPERATURE GRADIENTS

In Sec. IV, we have derived the connection condition to be used with the diffusion model and the fluid-dynamic equations. The remaining task is to obtain the transport coefficients $\mathcal{M}_P$ and $\mathcal{M}_T$ in the diffusion model. As we will

see, this amounts to computing the mass-flow rates of the pressure- and temperature-driven flows induced over a periodic cylinder array. We discuss these problems in this section.

A. Problem and relevant equations

We begin with the following problem. Let us consider a rarefied gas around infinitely many circular cylinders with radius r_c parallel to the X_3 axis (X_i is the space rectangular coordinates). The centers of the cylinders are located at $(X_1,X_2)=(mD,nD)$ $(m,n=0,\pm 1,\pm 2,\ldots)$, where D is the distance between the centers of adjacent cylinders. We consider the flow induced around the cylinders in two different physical situations, namely, the pressure-driven flow (P) and the temperature-driven flow (T):

(P) The gas is subject to a globally uniform pressure gradient in the X_1 direction. That is, the pressure is given by $p_0(1+C_P X_1/D)$ (C_P is a constant) in the absence of cylinders (or $r_c=0$). The cylinder surfaces are kept at a uniform and constant temperature T_0.

(T) The cylinder temperature is not uniform in the X_1 direction and is given by $T_0(1+C_T m)$ (C_T is a constant) for the cylinder whose center is located at $(X_1,X_2)=(mD,nD)$. There is no global pressure gradient.

Investigate the steady behavior of the gas on the basis of the BGK equation with the diffuse reflection boundary condition under the assumption that the constants C_P and C_T are so small that the problem can be linearized around the reference equilibrium state at rest with pressure p_0 and temperature T_0. Below, we attach the subscripts P and T to distinguish the quantities for the problems (P) and (T), respectively, and use α to designate P or T.

Let us introduce the following notations: $\rho_0=p_0/RT_0$ is the reference density, $\ell_0[=(2/\sqrt{\pi})(2RT_0)^{1/2}/A_c\rho_0]$ is the reference mean free path of the gas molecules, $K_0=\ell_0/D$ is the Knudsen number, $\hat{r}_c=r_c/D$, $x_i=X_i/D$, $(2RT_0)^{1/2}\zeta_i$ is the molecular velocity, $\rho_0(2RT_0)^{-3/2}(1+\tilde{\Phi}_\alpha)E(\boldsymbol{\zeta})$ is the velocity distribution function [$E(\boldsymbol{\zeta})$ is given by Eq. (55) with $\mathbf{c}=\boldsymbol{\zeta}$], $\rho_0(1+\tilde{\omega}_\alpha)$ is the density, $(2RT_0)^{1/2}\tilde{u}_{i\alpha}$ ($\tilde{u}_{3\alpha}=0$) is the flow velocity, $T_0(1+\tilde{\tau}_\alpha)$ is the temperature, and $p_0(1+\tilde{P}_\alpha)$ is the pressure of the gas. In addition, we denote by $\rho_0(2RT_0)^{1/2}C_\alpha D M_\alpha$ the mass-flow rate (per unit time) in the X_1 direction through a cross section $X_1=$const (with unit width in X_3 and with width D in X_2). According to Ref. 40, we can seek $\tilde{\Phi}_P$ and $\tilde{\Phi}_T$ in the form $\tilde{\Phi}_P=C_P[x_1+\Phi_P(x_1,x_2,\boldsymbol{\zeta})]$ and $\tilde{\Phi}_T=C_T[(\zeta_j^2-5/2)x_1+\Phi_T(x_1,x_2,\boldsymbol{\zeta})]$, where Φ_P and Φ_T are periodic in x_1 and x_2 with period 1. Then, Φ_P and Φ_T are governed by the following equation and boundary condition:

$$\zeta_1\frac{\partial\Phi_\alpha}{\partial x_1}+\zeta_2\frac{\partial\Phi_\alpha}{\partial x_2}=\frac{2}{\sqrt{\pi}}\frac{1}{K_0}(\Psi_\alpha-\Phi_\alpha)-I_\alpha \quad (\mathbf{x}\in X_f), \tag{121}$$

$$\Psi_\alpha=\omega_\alpha+2(\zeta_1 u_{1\alpha}+\zeta_2 u_{2\alpha})+(\zeta_j^2-3/2)\tau_\alpha, \tag{122}$$

$$\Phi_\alpha=\kappa_{w\alpha}+(\zeta_j^2-3/2)\tau_{w\alpha} \quad \text{for } \zeta_1 n_1+\zeta_2 n_2>0 \quad (\mathbf{x}\in S), \tag{123}$$

$$\kappa_{w\alpha}=-\frac{1}{2}\tau_{w\alpha}-2\sqrt{\pi}\int_{\zeta_1 n_1+\zeta_2 n_2<0}(\zeta_1 n_1+\zeta_2 n_2)\Phi_\alpha E(\boldsymbol{\zeta})d\boldsymbol{\zeta}, \tag{124}$$

$$\Phi_\alpha\text{: periodic} \quad (x_1=\pm 1/2, x_2=\pm 1/2), \tag{125}$$

where $\mathbf{x}=(x_1,x_2)$, X_f is the region occupied by the gas in the square unit cell $|x_1|\leqslant 1/2$ and $|x_2|\leqslant 1/2$ in the dimensionless (x_1,x_2) plane, ω_α, $u_{i\alpha}$, and τ_α in Eq. (122) are defined in Eqs. (128a)–(128c) below, S is the surface of the cylinder centered at $(x_1,x_2)=(0,0)$ with radius $\hat{r}_c$ in the (x_1,x_2) plane, n_i $(n_3=0)$ is the unit normal vector to S pointing to the gas, and the inhomogeneous terms I_P, I_T, τ_{wP}, and τ_{wT} are given by

$$I_P=\zeta_1, \quad I_T=\zeta_1(\zeta_j^2-5/2), \quad \tau_{wP}=0, \quad \tau_{wT}=-x_1. \tag{126}$$

Here, the range of x_i $(i=1,2)$ has been restricted to $|x_i|\leqslant 1/2$ by the periodic condition (125). It should be noted that the problem depends not only on K_0 but also on $\hat{r}_c$ through S.

The macroscopic quantities are expressed as follows:

$$\tilde{\omega}_P=C_P(x_1+\omega_P), \quad \tilde{\omega}_T=C_T(-x_1+\omega_T), \tag{127a}$$

$$\tilde{u}_{iP}=C_P u_{iP}, \quad \tilde{u}_{iT}=C_T u_{iT}, \tag{127b}$$

$$\tilde{\tau}_P=C_P\tau_P, \quad \tilde{\tau}_T=C_T(x_1+C_T\tau_T), \tag{127c}$$

$$\tilde{P}_P=C_P(x_1+P_P), \quad \tilde{P}_T=C_T P_T, \tag{127d}$$

where ω_α, $u_{i\alpha}$, τ_α, and P_α are given by

$$\omega_\alpha=\int\Phi_\alpha E(\boldsymbol{\zeta})d\boldsymbol{\zeta}, \tag{128a}$$

$$u_{i\alpha}=\int\zeta_i\Phi_\alpha E(\boldsymbol{\zeta})d\boldsymbol{\zeta}, \tag{128b}$$

$$\tau_\alpha=\frac{2}{3}\int\left(\zeta_j^2-\frac{3}{2}\right)\Phi_\alpha E(\boldsymbol{\zeta})d\boldsymbol{\zeta}, \tag{128c}$$

$$P_\alpha=\omega_\alpha+\tau_\alpha. \tag{128d}$$

The mass-flow rate M_α is given by

$$M_\alpha=\int_{-1/2}^{1/2}u_{1\alpha}|_{x_1=\text{const}}dx_2. \tag{129}$$

B. Transport coefficients

As readily seen, Eqs. (121)–(125) are essentially the same as Eqs. (51)–(54) if we take into account the correspondence between K_0 and K (and the inessential difference in the origin of x_1). Similarly, Eq. (129) corresponds to Eq. (69) that defines the transport coefficients. Therefore, we can derive the transport coefficients once we obtain the mass-flow rates for the problems (P) and (T).

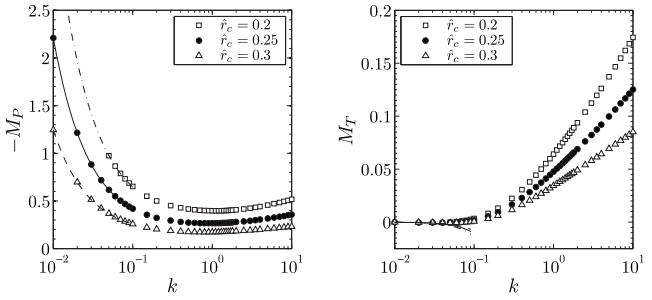

FIG. 4. The mass-flow rates M_P and M_T for $\hat{r}_c$=0.2, 0.25, and 0.3. The dashed-dotted line ($\hat{r}_c$=0.2), solid line ($\hat{r}_c$=0.25), and dashed line ($\hat{r}_c$=0.3) indicate the results obtained from the asymptotic expressions given in Refs. 39 and 40.

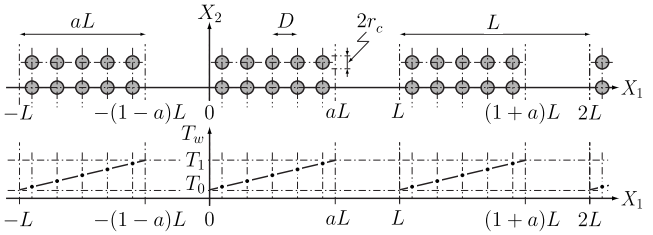

FIG. 5. An example of Kayashima's device composed of square arrays of circular cylinders and gaps. See the caption of Fig. 1.

The problems (P) and (T) governed by Eqs. (121)–(125) have been investigated in Refs. 39 and 40, and the features of the flows, especially that of the mass-flow rate, have been clarified. Therefore, we can make use of the numerical data for the mass-flow rates given in these references to derive the transport coefficients. In the present paper, however, in order to use more accurate numerical values, we repeated the same computations with higher accuracy. We also made additional computations to extend the range of available data with respect to the Knudsen number. The details of the present computations are left to Appendix.

We show the numerical results for M_P and M_T in Fig. 4 and in Table I. Here, the results are summarized using

$$k = \frac{\sqrt{\pi}}{2} K_0 \tag{130}$$

rather than K_0. This is because the computations have been carried out by specifying k instead of K_0. Finally, we conclude this section by the expression of the transport coefficients in terms of M_α. It is given by

$$\mathcal{M}_\alpha(K, \hat{r}_c) = M_\alpha\left(\frac{\sqrt{\pi}}{2} K, \hat{r}_c\right), \tag{131}$$

where the dependence on $\hat{r}_c$ has been explicitly shown.

VI. FLUID-DYNAMIC SYSTEM FOR A KNUDSEN-TYPE COMPRESSOR COMPOSED OF CYLINDER ARRAYS AND GAPS

Now we are ready to consider Kayashima's device having a long periodic structure composed of many cylinder arrays and gaps and to present its fluid-dynamic system. Let

TABLE I. Transport coefficients M_P and M_T for $\hat{r}_c$=0.2, 0.25, and 0.3. See the Appendix for the meaning of the values in the parentheses.

	$-M_P$			$M_T \times 10$				$-M_P$			$M_T \times 10$		
k	$\hat{r}_c$=0.2	$\hat{r}_c$=0.25	$\hat{r}_c$=0.3	$\hat{r}_c$=0.2	$\hat{r}_c$=0.25	$\hat{r}_c$=0.3	k	$\hat{r}_c$=0.2	$\hat{r}_c$=0.25	$\hat{r}_c$=0.3	$\hat{r}_c$=0.2	$\hat{r}_c$=0.25	$\hat{r}_c$=0.3
0.01	⋯	(2.2097)	(1.2456)	⋯	(−0.0011)	(−0.0008)	1.00	0.3965	0.2661	0.1734	0.6418	0.4768	0.3434
0.02	⋯	(1.2146)	(0.6973)	⋯	(−0.0033)	(−0.0028)	1.10	0.3963	0.2667	0.1741	0.6810	0.5052	0.3634
0.03	⋯	(0.8825)	(0.5145)	⋯	(−0.0052)	(−0.0049)	1.20	0.3965	0.2676	0.1749	0.7173	0.5314	0.3818
0.04	⋯	(0.7163)	(0.4230)	⋯	(−0.0059)	(−0.0062)	1.30	0.3971	0.2686	0.1758	0.7510	0.5557	0.3987
0.05	⋯	(0.6167)	(0.3680)	⋯	(−0.0049)	(−0.0065)	1.40	0.3980	0.2697	0.1767	0.7825	0.5785	0.4145
	0.9748	0.6166	0.3679	−0.0010	−0.0049	−0.0065	1.50	0.3991	0.2710	0.1776	0.8121	0.5998	0.4292
0.06	0.8661	0.5503	0.3312	0.0038	−0.0025	−0.0056	1.60	0.4004	0.2723	0.1786	0.8400	0.6199	0.4431
0.07	0.7889	0.5032	0.3050	0.0100	0.0012	−0.0037	1.70	0.4018	0.2737	0.1796	0.8664	0.6389	0.4561
0.08	0.7316	0.4680	0.2854	0.0173	0.0060	−0.0009	1.80	0.4032	0.2751	0.1806	0.8915	0.6569	0.4684
0.09	0.6873	0.4407	0.2702	0.0254	0.0116	0.0026	2.00	0.4064	0.2779	0.1826	0.9381	0.6904	0.4912
0.10	0.6522	0.4190	0.2581	0.0341	0.0178	0.0067	2.50	0.4151	0.2851	0.1875	1.0388	0.7626	0.5398
0.15	0.5491	0.3549	0.2217	0.0819	0.0539	0.0324	3.00	0.4240	0.2920	0.1920	1.1234	0.8230	0.5798
0.20	0.4992	0.3237	0.2040	0.1311	0.0925	0.0611	3.50	0.4327	0.2985	0.1962	1.1966	0.8749	0.6139
0.30	0.4509	0.2939	0.1870	0.2238	0.1652	0.1159	4.00	0.4411	0.3046	0.2001	1.2614	0.9207	0.6436
0.40	0.4279	0.2803	0.1795	0.3062	0.2287	0.1635	5.00	0.4567	0.3157	0.2071	1.3728	0.9987	0.6937
0.50	0.4150	0.2731	0.1757	0.3789	0.2837	0.2041	6.00	0.4709	0.3255	0.2132	1.4666	1.0638	0.7348
0.60	0.4072	0.2692	0.1738	0.4432	0.3317	0.2393	7.00	0.4838	0.3343	0.2186	1.5481	1.1197	0.7700
0.70	0.4023	0.2671	0.1730	0.5006	0.3740	0.2700	8.00	0.4956	0.3423	0.2234	1.6203	1.1690	0.8006
0.80	0.3992	0.2661	0.1728	0.5522	0.4117	0.2971	9.00	0.5064	0.3495	0.2278	1.6851	1.2129	0.8277
0.90	0.3974	0.2658	0.1730	0.5991	0.4458	0.3214	10.00	0.5164	0.3562	0.2318	1.7440	1.2527	0.8521

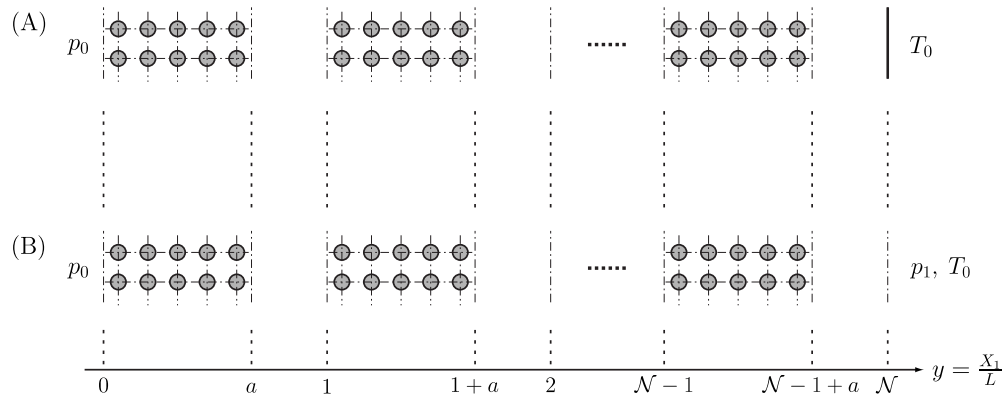

FIG. 6. Kayashima's device in two different situations. In case (A), the right end is closed by a wall with temperature T_0, whereas in case (B), both ends are open.

us consider a periodic structure consisting of many square arrays of circular cylinders and gaps, as shown in Fig. 5. More precisely, the cylinder arrays are located in $mL<X_1<(m+a)L$ $(m=0,\pm1,\pm2,\ldots;0<a<1)$ and they are separated by gaps with uniform distance $(1-a)L$. We shall call the union of a cylinder array and a gap a basic unit (or simply unit). We also call, in the basic unit, the part of the cylinder array subunit I and that of the gap subunit II. The length of one unit is therefore L. The common radius of the cylinders is r_c and the distance between the centers of neighboring cylinders is $D(>2r_c)$. In order to induce a flow thermally, we need to impose a temperature distribution on the cylinder arrays. This temperature distribution is described by $T_w(X_1)$, which is a periodic function of X_1 with period L. It is noted that T_w is defined for $mL<X_1<(m+a)L$ $(m=0,\pm1,\pm2,\ldots)$. Let us assume that the length of subunit I as well as that of subunit II is much larger than the distance between the centers of the cylinders D. Then, Eqs. (118) and (119) and the connection condition (120) describe the global behavior of the gas, i.e.,

$$\frac{\partial\hat{p}}{\partial\hat{t}}+\frac{\hat{T}_w}{(1-\pi\hat{r}_c^2)}\frac{\partial M}{\partial y}=0, \tag{132a}$$

$$M=\frac{\hat{p}}{\hat{T}_w^{1/2}}\left[\mathcal{M}_P(K,\hat{r}_c)\frac{\partial\ln\hat{p}}{\partial y}+\mathcal{M}_T(K,\hat{r}_c)\frac{d\ln\hat{T}_w}{dy}\right], \tag{132b}$$

$$K=K_*\hat{T}_w^{3/2}/\hat{p}$$

$$(m<y<m+a;m=0,\pm1,\pm2,\ldots), \tag{132c}$$

$$\frac{\partial\hat{p}}{\partial y}=0, \tag{133a}$$

$$\frac{\partial\hat{\rho}}{\partial\hat{t}}+\frac{\partial}{\partial y}(\hat{\rho}\hat{v}_1)=0, \tag{133b}$$

$$\frac{3}{2}\frac{\partial\hat{p}}{\partial\hat{t}}+\frac{\partial}{\partial y}\left(\frac{5}{2}\hat{p}\hat{v}_1-\frac{5}{4}k_*\hat{T}\frac{\partial\hat{T}}{\partial y}\right)=0, \tag{133c}$$

$$\hat{\rho}=\hat{p}/\hat{T}$$

$$(m+a<y<m+1;m=0,\pm1,\pm2,\ldots), \tag{133d}$$

$$\hat{p}\text{: continuous}, \tag{134a}$$

$$\hat{T}=\hat{T}_w,\quad M=\hat{\rho}\hat{v}_1$$

$$(y=m,m+a;m=0,\pm1,\pm2,\ldots). \tag{134b}$$

Here, L has been taken as the reference length and the dimensionless variables are the same as those in the preceding sections, but the subscript "(0)" of $\hat{p}$ and $\hat{T}$, and the subscript "(1)" of $\hat{v}_1$ are omitted. $\mathcal{M}_P$ and $\mathcal{M}_T$ are given by Eq. (131). It should be mentioned that similar fluid-dynamic systems have been constructed for the Knudsen compressor composed of pipes (or channels) in the case of a single-component gas[31,33] as well as in the case of a gas mixture.[49] It should also be mentioned that this approach has been initiated in Ref. 30 using a simplified BGK model in the context of the Knudsen pump. In Sec. VII, we analyze the flow in the present compressor numerically by applying the diffusion system (132)–(134).

VII. NUMERICAL RESULTS AND DISCUSSION

In this section, we show some numerical results for the fluid-dynamic system derived in the preceding sections. Hereafter, we assume that the global temperature distribution T_w is given by a linear function of X_1 in each subunit I, as shown in Fig. 5. To be more specific, let us set

$$T_w=\begin{cases}T_0 & (X_1=mL)\\ T_1 & (X_1=(m+a)L)\end{cases}$$
$$(m=0,\pm1,\pm2,\ldots;T_0<T_1). \tag{135}$$

Then, T_w in each subunit I is given by the line segment connecting T_0 and T_1.

Let us assume that the device is composed of $\mathcal{N}$ basic units and consider the flow in $0<X_1<\mathcal{N}L$. Following Refs. 31 and 35, we consider the following two situations (Fig. 6):

(A) The right end ($X_1=\mathcal{N}L$) of the device is closed by a wall kept at a uniform temperature T_0. The left end ($X_1=0$) is open and the gas pressure there is given by p_0.

(B) Both ends are open. The pressure at the left end ($X_1=0$) is kept at p_0, whereas that at the right end ($X_1=\mathcal{N}L$) at p_1. The temperature of the gas at the right end is T_0.

Case (A) estimates the pressure difference that can be maintained by the device, whereas case (B) estimates the flow rate produced by it against an imposed pressure difference.

Let us take T_0 and p_0 as the reference temperature and pressure, respectively, i.e., $T_*=T_0$ and $p_*=p_0$. Then, the parameters characterizing the present problems are T_1/T_0, r_c/D, a, $\mathcal{N}$, and K_* in case (A), and T_1/T_0, r_c/D, a, $\mathcal{N}$, K_*, and p_1/p_0 in case (B), where the Knudsen number K_* is defined by $K_*=\ell_*/D$, with $\ell_*=(2/\sqrt{\pi})(2RT_0)^{1/2}/A_c\rho_0$ being the mean free path of the gas molecules in the equilibrium state at rest with temperature T_0 and density $\rho_0=p_0/RT_0$. In the present study, we restrict ourselves to the steady state and solve the diffusion system (132)–(134) with $\partial\hat{p}/\partial\hat{t}=\partial\hat{\rho}/\partial\hat{t}=0$ in $0<y<\mathcal{N}$ by imposing the following boundary conditions:

$$\hat{p}=1 \quad (y=0), \tag{136a}$$

$$\hat{v}_1=0, \quad \hat{T}=1 \quad (y=\mathcal{N})$$

in case (A) and

$$\hat{p}=1 \quad (y=0), \tag{136b}$$

$$\hat{p}=p_1/p_0, \quad \hat{T}=1 \quad (y=\mathcal{N})$$

in case (B).

We first show the result for case (A) in Figs. 7–10. Figure 7 shows the steady pressure distribution $p/p_0(=\hat{p})$ in the case in which only a single unit is used ($\mathcal{N}=1$); Fig. 7(a) shows the effect of K_*, Fig. 7(b) that of r_c/D, Fig. 7(c) that of T_1/T_0, and Fig. 7(d) that of a. The pressure rise at the closed end ($y=1$) becomes larger with the increase of K_*, T_1/T_0, or r_c/D, and the pressure rise is almost independent of a. Among these features, the effects of K_*, T_1/T_0, and a remain unchanged when the number of the units is increased to a large number. On the other hand, as for the influence of r_c/D, a smaller r_c/D may give a higher pressure rise when $\mathcal{N}$ is large, as shown below.

Figures 8 and 9 show the steady pressure distributions when 100 units are used ($\mathcal{N}=100$). That is, Fig. 8(a) shows p/p_0 versus $y/\mathcal{N}$ for various K_* in the case of $r_c/D=0.25$, and Fig. 8(b) shows that for $r_c/D=0.2$, 0.25, and 0.3 in the case of $K_*=1$ ($a=0.5$ and $T_1/T_0=1.5$). Figure 9 is the corresponding figure for $T_1/T_0=2$. The pressure rise at the closed

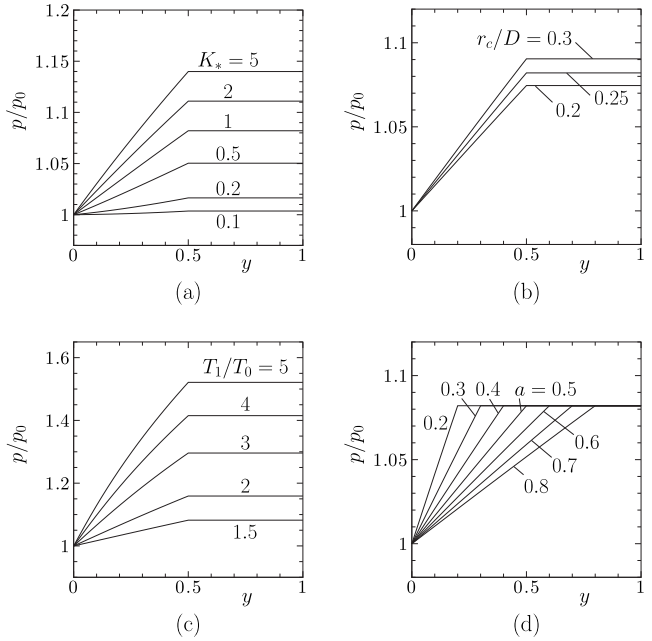

FIG. 7. p/p_0 vs y in case (A) for $\mathcal{N}=1$. (a) $T_1/T_0=1.5$, $r_c/D=0.25$, $a=0.5$, and $K_*=0.1$, 0.2, 0.5, 1, 2, and 5. (b) $T_1/T_0=1.5$, $K_*=1$, $a=0.5$, and $r_c/D=0.2$, 0.25, and 0.3. (c) $K_*=1$, $r_c/D=0.25$, $a=0.5$, and $T_1/T_0=1.5$, 2, 3, 4, and 5. (d) $T_1/T_0=1.5$, $K_*=1$, $r_c/D=0.25$, and $a=0.2$, 0.3, 0.4, 0.5, 0.6, 0.7, and 0.8.

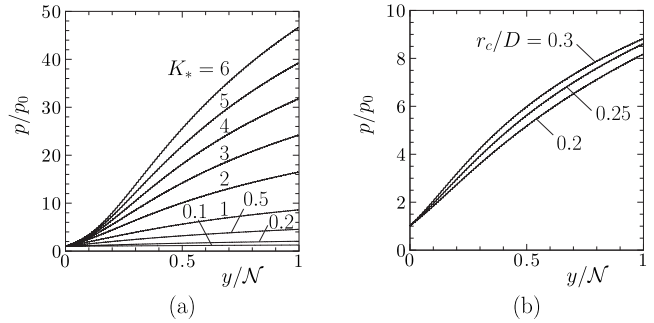

FIG. 8. p/p_0 vs $y/\mathcal{N}$ in case (A) for $\mathcal{N}=100$, $T_1/T_0=1.5$, and $a=0.5$. (a) $r_c/D=0.25$, and $K_*=0.1$, 0.2, 0.5, 1, 2, 3, 4, 5, and 6. (b) $K_*=1$, and $r_c/D=0.2$, 0.25, and 0.3.

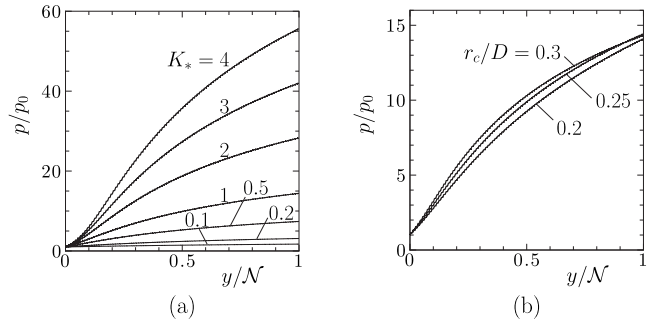

FIG. 9. p/p_0 vs $y/\mathcal{N}$ in case (A) for $\mathcal{N}=100$, $T_1/T_0=2$, and $a=0.5$. (a) $r_c/D=0.25$, and $K_*=0.1$, 0.2, 0.5, 1, 2, 3, and 4. (b) $K_*=1$, and $r_c/D=0.2$, 0.25, and 0.3.

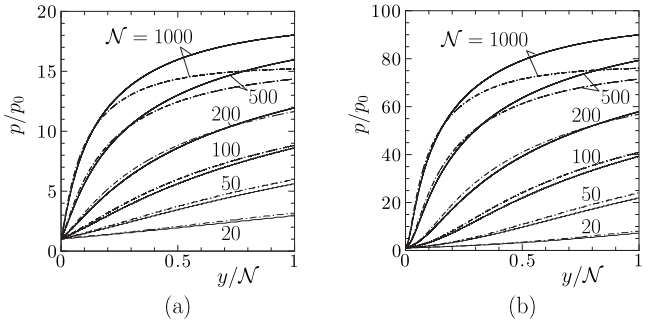

FIG. 10. p/p_0 vs $y/\mathcal{N}$ in case (A) for various $\mathcal{N}$ and for $r_c/D=0.25$ and 0.3 ($T_1/T_0=1.5$ and $a=0.5$). (a) $K_*=1$, (b) $K_*=5$. The solid line indicates the result for $r_c/D=0.25$ and the dashed-dotted line that for $r_c/D=0.3$.

end ($y=\mathcal{N}$) increases with K_*. In Fig. 8(b), larger r_c/D gives a higher pressure rise and the highest pressure rise is attained for $r_c/D=0.3$. On the other hand, in Fig. 9(b), the highest pressure rise is attained for $r_c/D=0.25$, and $r_c/D=0.3$ gives the second highest pressure rise.

Figure 10 contains further information on the effect of $\mathcal{N}$ on the pressure rise. That is, the pressure distributions for various numbers of the units ($\mathcal{N}=20$, 50, 100, 200, 500, and 1000) are shown for $r_c/D=0.25$ and 0.3 and for $K_*=1$ and 5 in the case of $T_1/T_0=1.5$ and $a=0.5$; Fig. 10(a) for $K_*=1$ and Fig. 10(b) for $K_*=5$. As $\mathcal{N}$ becomes large, the total pressure rise tends to approach a limiting value for each r_c/D. The limiting value is smaller for larger r_c/D. Owing to the difference in the limiting pressure rises, a smaller r_c/D can produce a higher pressure rise at the closed end when $\mathcal{N}$ is large.

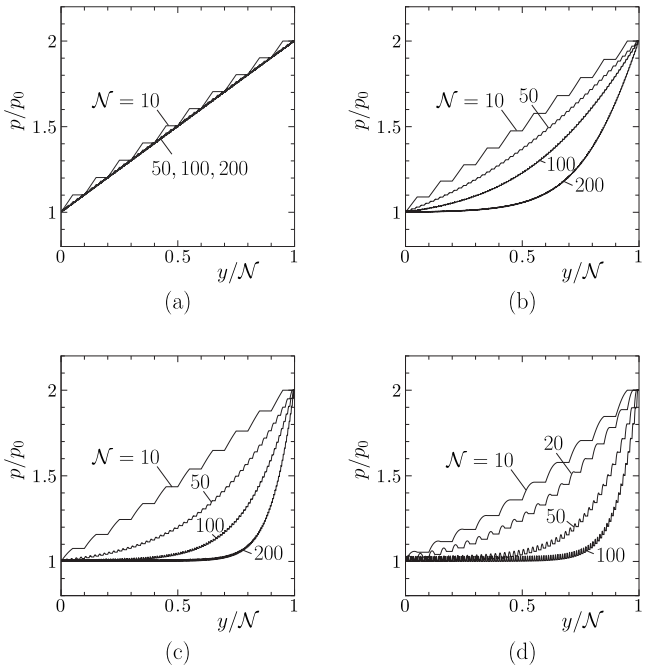

FIG. 11. p/p_0 vs $y/\mathcal{N}$ in case (B) for various $\mathcal{N}$ ($r_c/D=0.25$, $a=0.5$, $K_*=1$, and $p_1/p_0=2$). (a) $T_1/T_0=1$, (b) $T_1/T_0=1.5$, (c) $T_1/T_0=2$, and (d) $T_1/T_0=3$.

Figure 11 shows the steady pressure distribution $p/p_0(=\hat{p})$ versus $y/\mathcal{N}$ in case (B) for various $\mathcal{N}$ in the case of $T_1/T_0=1$, 1.5, 2, and 3 ($p_1/p_0=2$, $r_c/D=0.25$, $a=0.5$, and $K_*=1$); Fig. 11(a) for $T_1/T_0=1$, Fig. 11(b) for $T_1/T_0=1.5$, Fig. 11(c) for $T_1/T_0=2$, and Fig. 11(d) for $T_1/T_0=3$. The corresponding mass-flow rate M, which is constant in y (or X_1), is shown in Table II. When the global temperature distribution is uniform ($T_1/T_0=1$), an imposed pressure difference causes a leftward flow. This flow is reduced when a global temperature gradient is imposed on the cylinder arrays, which tries to drive a flow in the rightward direction. As the number of the units is increased, the temperature-driven flow overcomes the pressure-driven flow and a net flow in the rightward direction is obtained. The induced flow rate is larger for larger T_1/T_0. As $\mathcal{N}\to\infty$, the mass-flow rate tends to approach a limiting value for each T_1/T_0, irrespective of p_1/p_0 ($M\to 0$ for $T_1/T_0=1$). On the other hand, when $\mathcal{N}$ is large, the global pressure distribution becomes uniform, except in a narrow region (in $y/\mathcal{N}$) adjacent to the high pressure end. The thickness of the region becomes thinner as $\mathcal{N}$ is increased. These features are the same as those of the Knudsen compressor composed of channels[33] or pipes.[35]

VIII. CONCLUDING REMARKS

In this paper, we have considered a rarefied gas flow in Kayashima's device, composed of many periodic arrays of circular cylinders, for the case in which the channel is infinitely wide, and derived its diffusion model on the basis of the BGK equation and the diffuse reflection boundary condition.

This derivation involves several steps. In the first step, we considered a flow over a square array of parallel circular cylinders with a slowly varying temperature distribution. We derived a diffusion model that describes the pressure distribution and mass flux of the gas through the array by homogenization (Sec. II). This derivation also requires numerical data of the mass-flow rates of the pressure- and temperature-driven flows, which are available in previous literature. In the second step, we considered a slow flow across the gap and derived a set of fluid-dynamic equations that describes its overall behavior (Sec. III). In the third step, we considered the case in which the cylinder array is in contact with a half space filled with the gas (Sec. IV). On the basis of the diffusion model and the fluid-dynamic equations derived above, we derived the connection condition at the junction of the array and the gap. In Sec. V, the numerical values of the transport coefficients of the diffusion model are presented. The fluid-dynamic system for the entire periodic structure was summarized in Sec. VI. Finally, some numerical results for the model were presented in Sec. VII.

The derived model can be used as a convenient tool for estimating various properties of the device in both steady and unsteady conditions. Thus far, we have only considered one of the simplest cases of the porous media, namely, a square array of parallel circular cylinders. The present analysis can easily be extended to other types of porous media with a periodic structure. Such an extension will improve the applicability of the present model.

TABLE II. Dimensionless mass-flow rate M corresponding to Fig. 11.

	M					
	$p_1/p_0=1.5$		$p_1/p_0=2$			
$\mathcal{N}$	$T_1/T_0=1$	$T_1/T_0=1.5$	$T_1/T_0=1$	$T_1/T_0=1.5$	$T_1/T_0=2$	$T_1/T_0=3$
5	−5.343(−2)[a]	−5.685(−3)	−1.080(−1)	−5.119(−2)	−7.781(−3)	5.382(−2)
10	−2.672(−2)	1.813(−2)	−5.400(−2)	−3.485(−3)	3.576(−2)	9.147(−2)
20	−1.336(−2)	2.993(−2)	−2.700(−2)	2.026(−2)	5.685(−2)	1.075(−1)
50	−5.344(−3)	3.665(−2)	−1.080(−2)	3.404(−2)	6.726(−2)	1.120(−1)
100	−2.672(−3)	3.833(−2)	−5.401(−3)	3.784(−2)	6.850(−2)	1.121(−1)
200	−1.336(−3)	3.863(−2)	−2.701(−3)	3.868(−2)	6.857(−2)	⋯

[a]Read as -5.343×10^{-2}.

ACKNOWLEDGMENTS

The author expresses his cordial thanks to Professor Kazuo Aoki for his continuous encouragement and helpful discussions. He also thanks Professor Shigeru Takata for his valuable advices for the manuscript. The present work was supported by Grant-in-Aid for Young Scientists (B) (No. 19760118) from the Ministry of Education, Culture, Sports, Science and Technology (MEXT).

APPENDIX: DATA ON THE NUMERICAL COMPUTATION

The details on the numerical analysis of problems (121)–(125) are given in this appendix. Below, we use $k=(\sqrt{\pi}/2)K_0$ [Eq. (130)] instead of K_0.

1. Reduction of the problem

Let us introduce the heat-flow vector $p_0(2RT_0)^{1/2}C_\alpha Q_{i\alpha}$ $(Q_{3\alpha}=0)$ in addition to the macroscopic quantities already introduced in Sec. V, i.e.,

$$Q_{i\alpha}=\int \zeta_i\zeta_j^2\Phi_\alpha E(\boldsymbol{\zeta})d\boldsymbol{\zeta}-\frac{5}{2}u_{i\alpha}. \tag{A1}$$

From Eqs. (121)–(125), one can show that the following relation holds (the symmetric relation[57]):

$$M_T=\int_{X_f}Q_{1P}d\mathbf{x}+\int_S x_1(Q_{1P}n_1+Q_{2P}n_2)dl$$
$$=\int_{-1/2}^{1/2}Q_{1P}|_{x_1=1/2}dx_2, \tag{A2}$$

where $d\mathbf{x}=dx_1dx_2$ and dl is the line element along the cylinder surface S. The second equality is obtained by applying the divergence theorem. This type of relation is often referred to as the Onsager relation.[58–61] Equation (A2) shows that as far as the mass-flow rate M_T is concerned, it is obtained from the information on the heat flux Q_{iP} of the pressure-driven flow without solving the problem for Φ_T. Since our interest in this paper is M_T, we shall take the full advantage of this property; we only consider the problem of the pressure-driven flow [i.e., Eqs. (121)–(125) with $\alpha=P$] below and compute M_T from Q_{iP} using Eq. (A2). In this way, the amount of necessary computations is greatly reduced. Incidentally, the flow pattern of the temperature-driven flow has been obtained in Ref. 40.

2. Further transformation of Equations (121)–(125) with $\alpha=P$

a. Reduction of ζ_3

By the standard procedure,[2,62] one can eliminate the component ζ_3 of the molecular velocity from the system. Let us introduce the following marginals of Φ_P:

$$\bar{\Phi}_P=\begin{bmatrix}g\\h\end{bmatrix}=\int_{-\infty}^{\infty}\begin{bmatrix}1\\\zeta_3^2\end{bmatrix}\Phi_P\frac{e^{-\zeta_3^2}}{\sqrt{\pi}}d\zeta_3. \tag{A3}$$

Multiplying Eq. (121) (with $\alpha=P$) by $e^{-\zeta_3^2}/\sqrt{\pi}$ or $\zeta_3^2e^{-\zeta_3^2}/\sqrt{\pi}$ and integrating the result with respect to ζ_3 from $-\infty$ to ∞, we obtain a set of simultaneous equations for g and h,

$$\zeta_1\frac{\partial}{\partial x_1}\begin{bmatrix}g\\h\end{bmatrix}+\zeta_2\frac{\partial}{\partial x_2}\begin{bmatrix}g\\h\end{bmatrix}=\frac{1}{k}\begin{bmatrix}g_e-g\\h_e-h\end{bmatrix}-\frac{\zeta_1}{2}\begin{bmatrix}2\\1\end{bmatrix}\quad(\mathbf{x}\in X_f), \tag{A4}$$

$$\begin{bmatrix}g_e\\2h_e\end{bmatrix}=\begin{bmatrix}\omega_P+2u_{1P}\zeta_1+2u_{2P}\zeta_2+\tau_P(\zeta_1^2+\zeta_2^2-1)\\\omega_P+2u_{1P}\zeta_1+2u_{2P}\zeta_2+\tau_P(\zeta_1^2+\zeta_2^2)\end{bmatrix}, \tag{A5}$$

$$\omega_P=\frac{1}{\pi}\int_{-\infty}^{\infty}\int_{-\infty}^{\infty}ge^{-(\zeta_1^2+\zeta_2^2)}d\zeta_1d\zeta_2, \tag{A6a}$$

$$u_{iP}=\frac{1}{\pi}\int_{-\infty}^{\infty}\int_{-\infty}^{\infty}\zeta_ige^{-(\zeta_1^2+\zeta_2^2)}d\zeta_1d\zeta_2, \tag{A6b}$$

$$\tau_P=\frac{2}{3\pi}\int_{-\infty}^{\infty}\int_{-\infty}^{\infty}[(\zeta_1^2+\zeta_2^2)g+h]e^{-(\zeta_1^2+\zeta_2^2)}d\zeta_1d\zeta_2-\omega_P. \tag{A6c}$$

Similarly, from Eqs. (123)–(125), we obtain the following boundary conditions for g and h:

$$\begin{bmatrix} g \\ h \end{bmatrix} = \frac{\kappa_{wP}}{2}\begin{bmatrix} 2 \\ 1 \end{bmatrix} \quad \text{for } \zeta_1 n_1 + \zeta_2 n_2 > 0 \quad (\mathbf{x} \in S), \tag{A7}$$

$$\kappa_{wP} = -\frac{2}{\sqrt{\pi}} \int_{\zeta_1 n_1 + \zeta_2 n_2 < 0} (\zeta_1 n_1 + \zeta_2 n_2) g e^{-(\zeta_1^2+\zeta_2^2)} d\zeta_1 d\zeta_2, \tag{A8}$$

$$\bar{\Phi}_P: \text{periodic} \quad (x_1 = \pm 1/2, x_2 = \pm 1/2). \tag{A9}$$

Q_{iP} is expressed in terms of g and h as

$$Q_{iP} = \frac{1}{\pi}\int_{-\infty}^{\infty}\int_{-\infty}^{\infty} \zeta_i[(\zeta_1^2+\zeta_2^2)g + h]e^{-(\zeta_1^2+\zeta_2^2)} d\zeta_1 d\zeta_2 - \frac{5}{2}u_{iP}. \tag{A10}$$

Owing to the symmetry of the problem, we can further assume that the flow field (or $\bar{\Phi}_P$) is symmetric with respect to $x_2=0$ and antisymmetric with respect to $x_1=0$. Therefore, we can analyze the problem in the first quadrant of X_f (say, X_f^*) by imposing the following boundary conditions at $x_1=0$ and $1/2$ and $x_2=0$ and $1/2$:

$$\bar{\Phi}_P(0, x_2, \zeta_1, \zeta_2) = -\bar{\Phi}_P(0, x_2, -\zeta_1, \zeta_2) \quad \text{for } \zeta_1 > 0 \quad (\hat{r}_c < x_2 \leqslant 1/2), \tag{A11a}$$

$$\bar{\Phi}_P(1/2, x_2, \zeta_1, \zeta_2) = -\bar{\Phi}_P(1/2, x_2, -\zeta_1, \zeta_2) \quad \text{for } \zeta_1 < 0 \quad (0 \leqslant x_2 \leqslant 1/2), \tag{A11b}$$

$$\bar{\Phi}_P(x_1, 0, \zeta_1, \zeta_2) = \bar{\Phi}_P(x_1, 0, \zeta_1, -\zeta_2) \quad \text{for } \zeta_2 > 0 \quad (\hat{r}_c < x_1 \leqslant 1/2), \tag{A11c}$$

$$\bar{\Phi}_P(x_1, 1/2, \zeta_1, \zeta_2) = \bar{\Phi}_P(x_1, 1/2, \zeta_1, -\zeta_2) \quad \text{for } \zeta_2 < 0 \quad (0 \leqslant x_1 \leqslant 1/2). \tag{A11d}$$

For the sake of later use, we also write some of the equations in the polar coordinates. Let us introduce the following polar coordinate system (Fig. 12):

$$x_1 = r\cos\theta, \quad x_2 = r\sin\theta, \tag{A12a}$$

$$\zeta_1 = \zeta\cos(\theta + \theta_\zeta), \quad \zeta_2 = \zeta\sin(\theta + \theta_\zeta). \tag{A12b}$$

Here, $\hat{r}_c \leqslant r \leqslant r_D$, $0 \leqslant \theta \leqslant \pi/2$, $0 \leqslant \zeta < \infty$, $-\pi \leqslant \theta_\zeta \leqslant \pi$, and $r_D(<1/2)$ is a parameter related to the grid system introduced below. We denote the quantities expressed in the polar coordinates by putting the superscript $\sharp$ [e.g., $g = g^\sharp(r, \theta, \zeta, \theta_\zeta)$, $\omega_P = \omega_P^\sharp(r, \theta)$, etc.]. Then, Eqs. (A4)–(A8) are recast as follows:

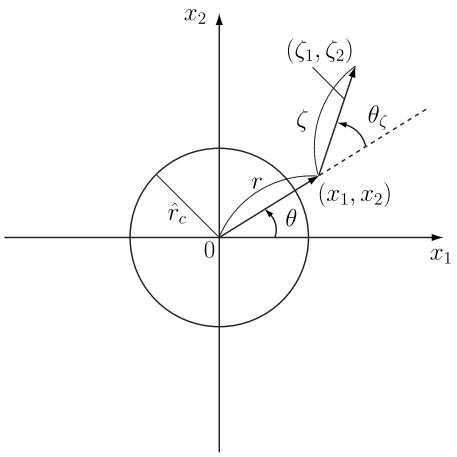

FIG. 12. Polar coordinate system.

$$\zeta\cos\theta_\zeta \frac{\partial}{\partial r}\begin{bmatrix} g^\sharp \\ h^\sharp \end{bmatrix} + \frac{\zeta\sin\theta_\zeta}{r}\left(\frac{\partial}{\partial\theta} - \frac{\partial}{\partial\theta_\zeta}\right)\begin{bmatrix} g^\sharp \\ h^\sharp \end{bmatrix} = \frac{1}{k}\begin{bmatrix} g_e^\sharp - g^\sharp \\ h_e^\sharp - h^\sharp \end{bmatrix} - \frac{\zeta\cos(\theta+\theta_\zeta)}{2}\begin{bmatrix} 2 \\ 1 \end{bmatrix}, \tag{A13}$$

$$\begin{bmatrix} g_e^\sharp \\ 2h_e^\sharp \end{bmatrix} = \begin{bmatrix} \omega_P^\sharp + 2\zeta(u_{rP}^\sharp\cos\theta_\zeta + u_{\theta P}^\sharp\sin\theta_\zeta) + \tau_P^\sharp(\zeta^2 - 1) \\ \omega_P^\sharp + 2\zeta(u_{rP}^\sharp\cos\theta_\zeta + u_{\theta P}^\sharp\sin\theta_\zeta) + \tau_P^\sharp\zeta^2 \end{bmatrix}, \tag{A14}$$

$$\omega_P^\sharp = \frac{1}{\pi}\int_{-\pi}^{\pi}\int_0^\infty \zeta g^\sharp e^{-\zeta^2} d\zeta d\theta_\zeta, \tag{A15a}$$

$$u_{rP}^\sharp = \frac{1}{\pi}\int_{-\pi}^{\pi}\int_0^\infty \zeta^2\cos\theta_\zeta g^\sharp e^{-\zeta^2} d\zeta d\theta_\zeta, \tag{A15b}$$

$$u_{\theta P}^\sharp = \frac{1}{\pi}\int_{-\pi}^{\pi}\int_0^\infty \zeta^2\sin\theta_\zeta g^\sharp e^{-\zeta^2} d\zeta d\theta_\zeta, \tag{A15c}$$

$$\tau_P^\sharp = \frac{2}{3\pi}\int_{-\pi}^{\pi}\int_0^\infty \zeta(\zeta^2 g^\sharp + h^\sharp)e^{-\zeta^2} d\zeta d\theta_\zeta - \omega_P^\sharp. \tag{A15d}$$

$$\begin{bmatrix} g^\sharp \\ h^\sharp \end{bmatrix} = \frac{\kappa_{wP}^\sharp}{2}\begin{bmatrix} 2 \\ 1 \end{bmatrix} \quad \text{for } -\frac{\pi}{2} < \theta_\zeta < \frac{\pi}{2} \quad (r = \hat{r}_c), \tag{A16}$$

$$\kappa_{wP}^\sharp = -\frac{2}{\sqrt{\pi}}\left(\int_{-\pi}^{-\pi/2} + \int_{\pi/2}^{\pi}\right)\int_0^\infty \zeta^2\cos\theta_\zeta g^\sharp e^{-\zeta^2} d\zeta d\theta_\zeta. \tag{A17}$$

The conditions corresponding to Eqs. (A11a) and (A11c) are

$$\bar{\Phi}_P^\sharp(r, \pi/2, \zeta, \theta_\zeta) = -\bar{\Phi}_P^\sharp(r, \pi/2, \zeta, -\theta_\zeta) \quad \text{for } -\pi < \theta_\zeta < 0, \tag{A18a}$$

$$\bar{\Phi}_P^\sharp(r, 0, \zeta, \theta_\zeta) = \bar{\Phi}_P^\sharp(r, 0, \zeta, -\theta_\zeta) \quad \text{for } 0 < \theta_\zeta < \pi \tag{A18b}$$

$(\hat{r}_c < r \leqslant r_D)$. The x_i component of the flow velocity is obtained from $(u_{rP}^\sharp, u_{\theta P}^\sharp)$ by

$$u_{1P}^{\sharp} = u_{rP}^{\sharp} \cos\theta - u_{\theta P}^{\sharp} \sin\theta, \tag{A19a}$$

$$u_{2P}^{\sharp} = u_{rP}^{\sharp} \sin\theta + u_{\theta P}^{\sharp} \cos\theta. \tag{A19b}$$

b. Integral equations

It is well known that the velocity distribution function is discontinuous around a convex boundary.[2,63] For the problem under consideration, a discontinuity leaving the cylinder surface is reflected at the boundary $x_1=0$ and $1/2$ and $x_2=0$ and $1/2$, according to condition (A11), and continues to propagate until it reaches the cylinder surface. To obtain $\bar{\Phi}_P$ having such a complicated structure by a direct method (e.g., finite-difference method) is a formidable task. To bypass this difficulty, we transform Eqs. (A4)–(A8) and (A11) into a set of linear integral equations for the macroscopic quantities (ω_P, u_{1P}, u_{2P}, τ_P, and κ_{wP}) by eliminating the velocity distribution function.[1,2] The resulting integral equations are given in Eqs. (65)–(67) of Ref. 39 (ω_P, u_{iP}, τ_P, κ_{wP}, $\mathbf{x}$, and X_f are denoted by ω, u_i, τ, κ_w, $\mathbf{y}$, and Y_f, respectively; see also the last paragraph of Sec. III A of the same reference). Similarly, we express Q_{iP} in terms of ω_P, u_{iP}, τ_P, and κ_{wP}. Since the expression is rather lengthy, we omit it here for brevity.

3. Numerical methods

a. Case of moderate and large *k*

For moderate and large k, the pressure-driven flow is analyzed on the basis of the integral equations. Similar integral equations have been solved in Ref. 64, where a two-dimensional rarefied gas flow confined in noncoaxial circular cylinders has been investigated. Therefore, we can exploit the method used in this reference by adapting it to the present problem. Since the detailed description is given there, we only outline the numerical method.

(i) Let us write the integral equations in the following symbolic form:

$$\mathbf{y} = A(\mathbf{y}) + \mathbf{b}, \tag{A20}$$

where $\mathbf{y}$ is the column vector composed of (ω_P, u_{1P}, u_{2P}, τ_P, κ_{wP}), $A(\mathbf{y})$ is the linear integral operator, and $\mathbf{b}$ is the column vector corresponding to the inhomogeneous terms. Equation (A20) is solved by the method of successive approximation. That is, we obtain the discrete solution $\mathbf{y}_\natural$ of $\mathbf{y}$ at the lattice points in the (x_1,x_2) plane as the limit of the sequence $\mathbf{y}_\natural^{(n)}$ $(n=0,1,\ldots)$ constructed by the formula

$$\mathbf{y}_\natural^{(n+1)} = A_\natural(\mathbf{y}_\natural^{(n)}) + \mathbf{b}_\natural, \tag{A21}$$

where $A_\natural$ and $\mathbf{b}_\natural$ are the discrete counterparts of A and $\mathbf{b}$, respectively.

(ii) $A(\mathbf{y})$ contains an area and a line integral in the (x_1,x_2) plane, whose domains of integration vary with point $\mathbf{x}$ in X_f^* (see Fig. 13). Similarly, $\mathbf{b}$ contains a line integral in the (x_1,x_2) plane. For the numerical integration, we first truncate the domain of integration by restricting the ranges of x_1 and x_2 to $|x_1| \le N_c+1/2$ and $|x_2| \le N_c+1/2$. Here, N_c is a sufficiently large positive integer. Then, the area and line integrals are evaluated numerically by using the Gauss–

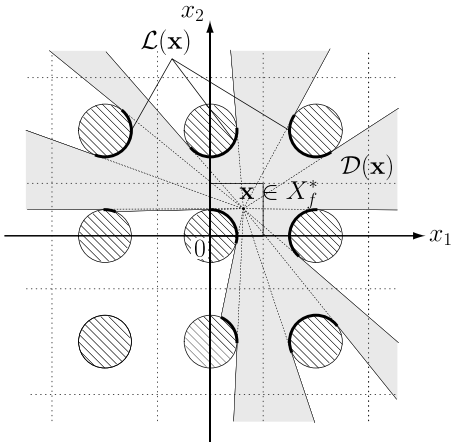

FIG. 13. The domain of integration. The domain of integration for the area integral, say $\mathcal{D}(\mathbf{x})$, is the region occupied by the gas visible from $\mathbf{x}$ and that for the line integral, say $\mathcal{L}(\mathbf{x})$, is the surfaces of the cylinders visible from $\mathbf{x}$.

Legendre quadrature, as described in Ref. 64. The values of N_c used in the present computations are summarized as follows:

$$\begin{cases} 2 \le N_c \le 4 & (0.05 \le k \le 0.15) \\ 6 \le N_c \le 10 & (0.2 \le k \le 0.6) \\ 12 \le N_c \le 18 & (0.7 \le k \le 1.6) \\ 20 \le N_c \le 29 & (1.7 \le k \le 2.5) \\ 35 \le N_c \le 49 & (3 \le k \le 7) \\ 56 \le N_c \le 70 & (8 \le k \le 10) \end{cases} \tag{A22}$$

for $\hat{r}_c=0.2$, 0.25, and 0.3.

(iii) The grid system used in the present computation is shown in Fig. 14. It is a composite grid system consisting of two subgrids I and II. Subgrid I is a rectangular grid system in the staircaselike domain ABCDEFGHA with steps at $x_1=b/2$ (BC) and $c/2$ (DE) and $x_2=b/2$ (CD) and $c/2$ (AB). It consists of uniformly distributed $(M+1)$ lattice lines both in the x_1 and x_2 directions (we choose the constants b and c in such a way that the segments AB, BC, CD, and DE are on

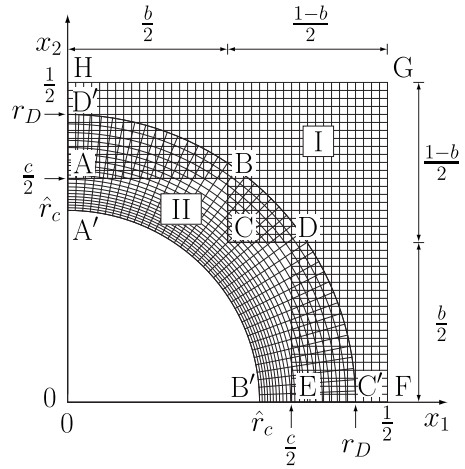

FIG. 14. Grid system consisting of two subgrids I and II. Subgrid I is a rectangular grid system in the staircaselike domain ABCDEFGHA and subgrid II is a polar grid system in the domain A′B′C′D′A′.

the lattice lines). Subgrid II is a polar grid system bounded by the cylinder surface (A′B′), the quarter circle C′D′ with radius r_D sharing the same center with the cylinder, the segment B′C′ on the x_1 axis, and the segment D′A′ on the x_2 axis. It consists of (M_r+1) nonuniformly distributed concentric quarter circles (finner near the inner cylinder and coarser near the outer) and $(M_\theta+1)$ uniformly distributed radial lines. The macroscopic quantities $(\omega_P, u_{1P}, u_{2P}, \tau_P, \kappa_{wP})$ are evaluated at each grid node in both subgrids. The grid parameters are summarized as follows. For subgrid I, $(M,b,c)=(40,4,5)$ for $\hat{r}_c=0.2$, $(M,b,c)=(40,4,6)$ for $\hat{r}_c=0.25$, and $(M,b,c)=(40,5,7)$ for $\hat{r}_c=0.3$ $(0.05\leqslant k\leqslant 10)$. For subgrid II, $(M_r,r_D)=(20,0.33)$ for $\hat{r}_c=0.2$, $(M_r,r_D)=(20,0.37)$ for $\hat{r}_c=0.25$, and $(M_r,r_D)=(20,0.45)$ for $\hat{r}_c=0.3$ $(0.05\leqslant k\leqslant 10)$. The minimum (maximum) grid interval in the radial direction in subgrid II is approximately 3.6×10^{-3} (1.3×10^{-2}) for $\hat{r}_c=0.2$, 3.3×10^{-3} (1.2×10^{-2}) for $\hat{r}_c=0.25$, and 4.1×10^{-3} (1.5×10^{-2}) for $\hat{r}_c=0.3$. As for M_θ, $M_\theta=80$ $(0.05\leqslant k\leqslant 0.2)$ and $M_\theta=40$ $(0.3\leqslant k\leqslant 10)$ for $\hat{r}_c=0.2$ and 0.25, and $M_\theta=80$ $(0.05\leqslant k\leqslant 0.4)$ and $M_\theta=40$ $(0.5\leqslant k\leqslant 10)$ for $\hat{r}_c=0.3$.

b. Case of small *k*

When k is small, the discontinuity in the velocity distribution function is confined in a thin layer (the S layer[63]) adjacent to the boundary, and we can expect that the overall flow field is obtained accurately by a direct finite-difference analysis of Eqs. (A4)–(A8) and (A11) (neglecting the discontinuity). Since the finite-difference analysis is rather easy and efficient, we employ it for the analysis of the pressure-driven flow for small k ($k\leqslant 0.05$ in the actual computation). The values of M_P and M_T obtained by this method are shown in Table I in the parentheses. Below, we outline the solution method.

(i) We use the same grid system as before for the discretization in the (x_1,x_2) space (see the previous subsection). In subgrid I, we solve Eqs. (A4)–(A6) with the boundary condition (A11), supplemented by a boundary condition on ABCDE [Eq. (A23) below]. In subgrid II, we solve Eqs. (A13)–(A15) with the boundary conditions (A16)–(A18), supplemented by a boundary condition on C′D′ [Eq. (A24) below]. Since the velocity distribution function should be continuous in the gas, we impose the following condition on ABCDE:

$$\bar{\Phi}_P=\bar{\Phi}_P^\sharp \quad \text{for } \zeta_2>0 \quad \text{(on AB and CD)}, \tag{A23a}$$

$$\bar{\Phi}_P=\bar{\Phi}_P^\sharp \quad \text{for } \zeta_1>0 \quad \text{(on BC and DE)}, \tag{A23b}$$

and on C′D′,

$$\bar{\Phi}_P^\sharp=\bar{\Phi}_P \quad \text{for } -\pi<\theta_\zeta<-\frac{\pi}{2} \quad \text{and} \quad \frac{\pi}{2}<\theta_\zeta<\pi. \tag{A24}$$

(ii) We obtain the discrete solutions in both subgrids as the limits of the sequences constructed from a finite-difference scheme in each subgrid, which are expected to converge simultaneously. More precisely, in subgrid I, we try to obtain the discrete solution $\bar{\Phi}_{P\natural}$ of $\bar{\Phi}_P$ at the lattice points in the $(x_1,x_2,\zeta_1,\zeta_2)$ space as the limit of the sequence $\bar{\Phi}_{P\natural}^{(n)}$ $(n=0,1,\ldots)$ constructed by using a finite-difference scheme corresponding to Eq. (A4), giving the relation between $\bar{\Phi}_{P\natural}^{(n)}$ and $\bar{\Phi}_{P\natural}^{(n-1)}$. In subgrid II, we try to obtain the discrete solution $\bar{\Phi}_{P\natural}^\sharp$ of $\bar{\Phi}_P^\sharp$ at the lattice points in the $(r,\theta,\zeta,\theta_\zeta)$ space as the limit of the sequence $\bar{\Phi}_{P\natural}^{\sharp(n)}$ $(n=0,1,\ldots)$ constructed by using a finite-difference scheme corresponding to Eq. (A13), giving the relation between $\bar{\Phi}_{P\natural}^{\sharp(n)}$ and $\bar{\Phi}_{P\natural}^{\sharp(n-1)}$. $\bar{\Phi}_{P\natural}^{(n)}$ and $\bar{\Phi}_{P\natural}^{\sharp(n)}$ are related to each other through conditions (A23) and (A24). If $\bar{\Phi}_{P\natural}^{(n)}$ and $\bar{\Phi}_{P\natural}^{\sharp(n)}$ converge simultaneously, we take the limiting functions as the solutions $\bar{\Phi}_{P\natural}$ and $\bar{\Phi}_{P\natural}^\sharp$, respectively.

(iii) Let $\bar{\Phi}_{P\natural}^{(n-1)}$ and $\bar{\Phi}_{P\natural}^{\sharp(n-1)}$ be known. The process to obtain $\bar{\Phi}_{P\natural}^{(n)}$ and $\bar{\Phi}_{P\natural}^{\sharp(n)}$ are as follows. First, we obtain the boundary data of $\bar{\Phi}_{P\natural}^{\sharp(n)}$ on C′D′ from $\bar{\Phi}_{P\natural}^{(n-1)}$ by the interpolation. Let $\zeta_\natural$ and $\theta_{\zeta\natural}$ be the discrete sets for the variables ζ and θ_ζ, respectively. For $\pi/2\leqslant\theta_{\zeta\natural}\leqslant\pi$ (or for $-\pi\leqslant\theta_{\zeta\natural}\leqslant-\pi/2$), $\bar{\Phi}_{P\natural}^{\sharp(n)}$ is determined from $r=r_D$ to $\hat{r}_c$ and from $\theta=0$ to $\pi/2$ (or from $\theta=\pi/2$ to 0) in the descending (or ascending) order of $\theta_{\zeta\natural}$ by using the finite-difference equation, the boundary conditions on C′D′, and the boundary condition on B′C′ (or that on D′A′) for all $\zeta_\natural$. Similarly, for $0\leqslant\theta_{\zeta\natural}<\pi/2$ (or for $-\pi/2<\theta_{\zeta\natural}<0$), $\bar{\Phi}_{P\natural}^{\sharp(n)}$ is determined from $r=\hat{r}_c$ to r_D and from $\theta=0$ to $\pi/2$ (or from $\theta=\pi/2$ to 0) in the descending (or ascending) order of $\theta_{\zeta\natural}$ by using the finite-difference equation, the boundary conditions on A′B′, and the boundary condition on B′C′ (or that on D′A′) for all $\zeta_\natural$. Next, we obtain the boundary data of $\bar{\Phi}_{P\natural}^{(n)}$ on ABCDE from $\bar{\Phi}_{P\natural}^{\sharp(n)}$ by the interpolation. Let $\zeta_{1\natural}$ and $\zeta_{2\natural}$ be the discrete sets for the variables ζ_1 and ζ_2, respectively. For each $\zeta_{1\natural}\geqslant 0$, $\bar{\Phi}_{P\natural}^{(n)}$ is determined first from $x_1=0$ to $b/2$ and from $x_2=c/2$ to $1/2$ (or from $x_2=1/2$ to $c/2$), second from $x_1=b/2$ to $c/2$ and from $x_2=b/2$ to $1/2$ (or from $x_2=1/2$ to $b/2$), and finally from $x_1=c/2$ to $1/2$ and from $x_2=0$ to $1/2$ (or from $x_2=1/2$ to 0) by using the finite-difference equation, the boundary conditions on HA, BC, and DE, and the boundary conditions on AB, CD, and EF (or that on GH) for all $\zeta_{2\natural}\geqslant 0$ (or for all $\zeta_{2\natural}<0$). Similarly, for each $\zeta_{1\natural}<0$, $\bar{\Phi}_{P\natural}^{(n)}$ is determined first from $x_1=1/2$ to $c/2$ and from $x_2=0$ to $1/2$ (or from $x_2=1/2$ to 0), second from $x_1=c/2$ to $b/2$ and from $x_2=b/2$ to $1/2$ (or from $x_2=1/2$ to $b/2$), and finally from $x_1=b/2$ to 0 and from $x_2=c/2$ to $1/2$ (or from $x_2=1/2$ to $c/2$) by using the finite-difference equation, the boundary condition on FG, and the boundary conditions on EF, CD, and AB (or that on GH) for all $\zeta_{2\natural}\geqslant 0$ (or for all $\zeta_{2\natural}<0$).

(iv) The grid parameters are summarized here. For subgrid I, $(M,b,c)=(80,4,6)$ for $\hat{r}_c=0.25$, and $(M,b,c)=(80,5,7)$ for $\hat{r}_c=0.3$ $(0.01\leqslant k\leqslant 0.05)$. For subgrid II, $(M_r,r_D,M_\theta)=(60,0.45,80)$ for $\hat{r}_c=0.25$, and $(M_r,r_D,M_\theta)=(60,0.475,80)$ for $\hat{r}_c=0.3$ $(0.01\leqslant k\leqslant 0.05)$. The minimum (maximum) grid interval in the radial direction in subgrid II is approximately 1.8×10^{-3} (6.8×10^{-3}) for $\hat{r}_c=0.25$ and 1.6×10^{-3} (6.0×10^{-2}) for $\hat{r}_c=0.3$. As for the molecular velocity space (ζ,θ_ζ), we first restrict ζ in the range $0\leqslant\zeta\leqslant Z$

($Z \simeq 6.6$). Then, the space is subdivided by 61×321 ($\zeta \times \theta_\zeta$) lattice lines. The lattice lines for ζ are nonuniform (finner near $\zeta=0$) and those for θ_ζ are uniform. For the (ζ_1, ζ_2) space, we first express it by the polar coordinates, i.e., $\zeta_1 = \hat{\zeta} \cos \hat{\theta}_\zeta$ and $\zeta_2 = \hat{\zeta} \sin \hat{\theta}_\zeta$ ($0 < \hat{\zeta} < \infty$ and $-\pi \leqslant \hat{\theta}_\zeta \leqslant \pi$). Then, the $(\hat{\zeta}, \hat{\theta}_\zeta)$ space, restricted to $0 \leqslant \hat{\zeta} \leqslant Z$, is subdivided by 61×321 ($\hat{\zeta} \times \hat{\theta}_\zeta$) lattice lines in the same way as the (ζ, θ_ζ) space. The minimum (maximum) interval of the lattice lines for ζ (or $\hat{\zeta}$) is approximately 2.0×10^{-3} (0.29).

4. Data on accuracy

The simplest measure of accuracy is given by the uniformity of the mass-flow rate. That is, M_P should be theoretically independent of x_1, but it exhibits a slight variation owing to the numerical error. Let us denote by M_P^* the value of M_P shown in Table I. They are the values evaluated at $x_1 = 1/2$. As an accuracy test, we also evaluate M_P at each location of the lattice lines $x_1 = \text{const}$ constituting subgrid I and examine its unifomity. The result is summarized below. For the numerical solutions of the integral equations, the deviation of M_P from M_P^* is

$$\left| \frac{M_P - M_P^*}{M_P^*} \right| \leqslant \begin{cases} 4.1 \times 10^{-5} & (0.05 \leqslant k \leqslant 0.4) \\ 1.7 \times 10^{-4} & (0.5 \leqslant k \leqslant 2) \\ 6.8 \times 10^{-4} & (2.5 \leqslant k \leqslant 10) \end{cases} \tag{A25a}$$

for $\hat{r}_c = 0.2$,

$$\left| \frac{M_P - M_P^*}{M_P^*} \right| \leqslant \begin{cases} 5.3 \times 10^{-5} & (0.05 \leqslant k \leqslant 0.4) \\ 1.6 \times 10^{-4} & (0.5 \leqslant k \leqslant 2) \\ 3.2 \times 10^{-4} & (2.5 \leqslant k \leqslant 10) \end{cases} \tag{A25b}$$

for $\hat{r}_c = 0.25$, and

$$\left| \frac{M_P - M_P^*}{M_P^*} \right| \leqslant \begin{cases} 8.9 \times 10^{-5} & (0.05 \leqslant k \leqslant 0.4) \\ 3.1 \times 10^{-4} & (0.5 \leqslant k \leqslant 2) \\ 7.6 \times 10^{-4} & (2.5 \leqslant k \leqslant 10) \end{cases} \tag{A25c}$$

for $\hat{r}_c = 0.3$. For the numerical solutions obtained by the finite-difference analysis, the variation of M_P is

$$\left| \frac{M_P - M_P^*}{M_P^*} \right| \leqslant \begin{cases} 7.7 \times 10^{-5} & (\hat{r}_c = 0.25) \\ 1.1 \times 10^{-4} & (\hat{r}_c = 0.3) \end{cases} \tag{A26}$$

for $0.01 \leqslant k \leqslant 0.05$.

[1] C. Cercignani, *The Boltzmann Equation and Its Applications* (Springer-Verlag, Berlin, 1988).
[2] Y. Sone, *Molecular Gas Dynamics: Theory, Techniques, and Applications* (Birkhäuser, Boston, 2007). Supplementary Notes and Errata: Kyoto University Research Information Repository (http://hdl.handle.net/2433/66098).
[3] Y. Sone, "Flows induced by thermal stress in rarefied gas," Phys. Fluids **15**, 1418 (1972).
[4] Y. Sone, "Flows induced by temperature fields in a rarefied gas and their ghost effect on the behavior of a gas in the continuum limit," Annu. Rev. Fluid Mech. **32**, 779 (2000).
[5] M. N. Kogan, V. S. Galkin, and O. G. Fridlender, "Stresses produced in gases by temperature and concentration inhomogeneities. New type of free convection," Sov. Phys. Usp. **19**, 420 (1976).
[6] K. Aoki, Y. Sone, and N. Masukawa, in *Rarefied Gas Dynamics*, edited by J. Harvey and G. Lord (Oxford University Press, Oxford, 1995), pp. 35–41.
[7] Y. Sone and M. Yoshimoto, "Demonstration of a rarefied gas flow induced near the edge of a uniformly heated plate," Phys. Fluids **9**, 3530 (1997).
[8] E. H. Kennard, *Kinetic Theory of Gases* (McGraw-Hill, New York, 1938).
[9] Y. Sone, "Thermal creep in rarefied gas," J. Phys. Soc. Jpn. **21**, 1836 (1966).
[10] Y. Sone and K. Yamamoto, "Flow of rarefied gas through a circular pipe," Phys. Fluids **11**, 1672 (1968); **13**, 1651(E) (1970).
[11] S. K. Loyalka, "Thermal transpiration in a cylindrical tube," Phys. Fluids **12**, 2301 (1969).
[12] T. Ohwada, Y. Sone, and K. Aoki, "Numerical analysis of the shear and thermal creep flows of a rarefied gas over a plane wall on the basis of the linearized Boltzmann equation for hard-sphere molecules," Phys. Fluids A **1**, 1588 (1989).
[13] T. Ohwada, Y. Sone, and K. Aoki, "Numerical analysis of the Poiseuille and thermal transpiration flows between two parallel plates on the basis of the Boltzmann equation for hard-sphere molecules," Phys. Fluids A **1**, 2042 (1989); **2**, 639(E) (1990).
[14] F. Sharipov and V. Seleznev, "Data on internal rarefied gas flows," J. Phys. Chem. Ref. Data **27**, 657 (1998).
[15] F. Sharipov, "Application of the Cercignani-Lampis scattering kernel to calculations of rarefied gas flows. I. Plane flow between two parallel plates," Eur. J. Mech. B/Fluids **21**, 113 (2002).
[16] F. Sharipov, "Application of the Cercignani-Lampis scattering kernel to calculations of rarefied gas flows. III. Poiseuille flow and thermal creep through a long tube," Eur. J. Mech. B/Fluids **22**, 145 (2002).
[17] C.-C. Chen, I.-K. Chen, T.-P. Liu, and Y. Sone, "Thermal transpiration for the linearized Boltzmann equation," Commun. Pure Appl. Math. **60**, 147 (2007).
[18] C. E. Siewert, "The linearized Boltzmann equation: Concise and accurate solutions to basic flow problems," ZAMP **54**, 273 (2003).
[19] R. D. M. Garcia and C. E. Siewert, "The linearized Boltzmann equation with Cercignani-Lampis boundary conditions: Basic flow problems in a plane channel," Eur. J. Mech. B/Fluids **28**, 387 (2009).
[20] M. Knudsen, "Eine Revision der Gleichgewichtsbedingung der Gase. Thermische Molekularströmung," Ann. Phys. **31**, 205 (1910).
[21] M. Knudsen, "Thermischer Molekulardruck der Gase in Röhren," Ann. Phys. **33**, 1435 (1910).
[22] G. Pham-Van-Diep, P. Keeley, E. P. Muntz, and D. P. Weaver, in *Rarefied Gas Dynamics*, edited by J. Harvey and G. Lord (Oxford University Press, Oxford, 1995), pp. 715–721.
[23] Y. Sone, Y. Waniguchi, and K. Aoki, "One-way flow of a rarefied gas induced in a channel with a periodic temperature distribution," Phys. Fluids **8**, 2227 (1996).
[24] S. E. Vargo and E. P. Muntz, in *Rarefied Gas Dynamics*, edited by C. Shen (Peking University Press, Peking, 1997), pp. 995–1000.
[25] M. L. Hudson and T. J. Bartel, in *Rarefied Gas Dynamics*, edited by R. Brun, R. Campargue, R. Gatignol, and J.-C. Lengrand (Cépaduès-Éditions, Toulouse, 1999), Vol. 1, p. 719.
[26] Y. Sone and K. Sato, "Demonstration of a one-way flow of a rarefied gas induced through a pipe without average pressure and temperature gradients," Phys. Fluids **12**, 1864 (2000).
[27] K. Aoki, Y. Sone, S. Takata, K. Takahashi, and G. A. Bird, in *Rarefied Gas Dynamics*, edited by T. J. Bartel and M. A. Gallis (AIP, Melville, 2001), p. 940.
[28] Y. Sone, T. Fukuda, T. Hokazono, and H. Sugimoto, in *Rarefied Gas Dynamics*, edited by T. J. Bartel and M. A. Gallis (AIP, Melville, 2001), p. 948.
[29] Y. Sone and H. Sugimoto, in *Rarefied Gas Dynamics*, edited by A. D. Ketsdever and E. P. Muntz (AIP, Melville, 2003), pp. 1041–1048.
[30] K. Aoki and P. Degond, "Homogenization of a flow in a periodic channel of small section," Multiscale Model. Simul. **1**, 304 (2003).
[31] K. Aoki, P. Degond, S. Takata, and H. Yoshida, "Diffusion models for Knudsen compressors," Phys. Fluids **19**, 117103 (2007).
[32] K. Aoki, P. Degond, L. Mieussens, M. Nishioka, and S. Takata, in *Rarefied Gas Dynamics*, edited by M. S. Ivanov and A. K. Rebrov (Siberian Branch of the Russian Academy of Sciences, Novosibirsk, 2007), pp. 1079–1084.
[33] K. Aoki, P. Degond, L. Mieussens, S. Takata, and H. Yoshida, "A diffusion

model for rarefied flows in curved channels," Multiscale Model. Simul. **6**, 1281 (2008).
[34]K. Aoki, P. Degond, and L. Mieussens, "Numerical simulations of rarefied gases in curved channels: Thermal creep, circulating flow, and pumping effect," Comm. Comp. Phys. **6**, 919 (2009).
[35]K. Aoki, S. Takata, and K. Kugimoto, in *Rarefied Gas Dynamics*, edited by T. Abe (AIP, Melville, 2009), pp. 953–958.
[36]H. Sugimoto and Y. Sone, in *Rarefied Gas Dynamics*, edited by M. Capitelli (AIP, Melville, 2005), pp. 168–173.
[37]H. Sugimoto, "Numerical analysis of the rarefied flow in a vacuum pump driven by thermal edge flow," J. Vac. Soc. Jpn. **49**, 481 (2006).
[38]M. Kayashima, "Device for the transport and compression of gases by the use of the porous media," Japan Patent No. 1513106 (8 November 1988).
[39]S. Taguchi and P. Charrier, "Rarefied gas flow over an in-line array of circular cylinders," Phys. Fluids **20**, 067103 (2008); Phys. Fluids **20**, 119901(E) (2008).
[40]S. Taguchi, in *Rarefied Gas Dynamics*, edited by T. Abe (AIP, Melville, 2009), pp. 447–452.
[41]P. L. Bhatnagar, E. P. Gross, and M. Krook, "A model for collision processes in gases. I. Small amplitude processes in charged and neutral one-component systems," Phys. Rev. **94**, 511 (1954).
[42]P. Welander, "On the temperature jump in a rarefied gas," Ark. Fys. **7**, 507 (1954).
[43]P. Charrier and B. Dubroca, "Asymptotic transport models for heat and mass transfer in reactive porous media," Multiscale Model. Simul. **2**, 124 (2003).
[44]Y. Sone, in *Rarefied Gas Dynamics*, edited by L. Trilling and H. Y. Wachman (Academic, New York, 1969), Vol. 1, pp. 243–253.
[45]Y. Sone, in *Rarefied Gas Dynamics*, edited by D. Dini (Editrice Tecnico Scientfica, Pisa, 1971), Vol. 2, pp. 737–749.
[46]Y. Sone, in *Advances in Kinetic Theory and Continuum Mechanics*, edited by R. Gatignol and Soubbaramayer (Springer-Verlag, Berlin, 1991), pp. 19–31.
[47]Y. Sone, K. Aoki, S. Takata, H. Sugimoto, and A. V. Bobylev, "Inappropriateness of the heat-conduction equation for description of a temperature field of a stationary gas in the continuum limit: Examination by asymptotic analysis and numerical computation of the Boltzmann equation," Phys. Fluids **8**, 628 (1996); **8**, 841(E) (1996).
[48]Y. Sone, *Kinetic Theory and Fluid Dynamics* (Birkhäuser, Boston, 2002). Supplementary Notes and Errata: Kyoto University Research Information Repository (http://hdl.handle.net/2433/66099).
[49]S. Takata, H. Sugimoto, and S. Kosuge, "Gas separation by means of the Knudsen compressor," Eur. J. Mech. B/Fluids **26**, 155 (2007).
[50]S. Fukui and R. Kaneko, "Analysis of ultra-thin gas film lubrication based on linearized Boltzmann equation: First report—Derivation of a generalized lubrication equation including thermal creep flow," J. Tribol. **110**, 253 (1988).
[51]F. Sharipov, "Rarefied gas flow through a long tube at any temperature ratio," J. Vac. Sci. Technol. A **14**, 2627 (1996).
[52]F. Sharipov, "Rarefied gas flow through a long tube at arbitrary pressure and temperature drops," J. Vac. Sci. Technol. A **15**, 2434 (1997).
[53]C. Shen, "Use of the degenerated Reynolds equation in solving the microchannel flow problem," Phys. Fluids **17**, 046101 (2005).
[54]G. L. Vignoles, P. Charrier, C. Preux, and B. Dubroca, "Rarefied pure gas transport in non-isothermal porous media: Validation and tests of the model," Transp. Porous Media **75**, 295 (2008).
[55]C. Bardos, L. Dumas, and F. Golse, "Diffusion approximation for billiards with totally accommodating scatters," J. Stat. Phys. **86**, 351 (1997).
[56]For the present geometry, the velocity distribution function is generally discontinuous on the cylinder surface for the molecular velocity tangential to the surface. This discontinuity propagates into the gas along the characteristic of Eq. (83) and may reach the location of the junction. Therefore, precisely speaking, condition (90) is not applied across such a discontinuity in the gas. But even in this case, each limiting value in Eq. (90) should be continuous along the characteristic.
[57]S. Takata, "Symmetry of the linearized Boltzmann equation and its application," J. Stat. Phys. **136**, 751 (2009).
[58]F. Sharipov, "Onsager–Casimir reciprocity relations for open gaseous systems at arbitrary rarefaction I. General theory for single gas," Physica A **203**, 437 (1994).
[59]F. Sharipov, "Onsager–Casimir reciprocity relations for open gaseous systems at arbitrary rarefaction II. Application of the theory for single gas," Physica A **203**, 457–485 (1994).
[60]F. Sharipov, "Onsager–Casimir reciprocal relations based on the Boltzmann equation and gas-surface interaction: Single gas," Phys. Rev. E **73**, 026110 (2006).
[61]S. Takata, "Symmetry of the linearized Boltzmann equation. II. Entropy production and Onsager-Casimir relation," J. Stat. Phys. **136**, 945 (2009).
[62]C. K. Chu, "Kinetic-theoretic description of the formation of a shock wave," Phys. Fluids **8**, 12 (1965).
[63]Y. Sone and S. Takata, "Discontinuity of the velocity distribution function in a rarefied gas around a convex body and the S layer at the bottom of the Knudsen layer," Transp. Theory Stat. Phys. **21**, 501 (1992).
[64]K. Aoki, Y. Sone, and T. Yano, "Numerical analysis of a flow induced in a rarefied gas between noncoaxial circular cylinders with different temperatures for the entire range of the Knudsen number," Phys. Fluids A **1**, 409 (1989).